JOURNAL OF GEOPHYSICAL RESEARCH, VOL. 106, NO. D1, PAGES 1113–1138, JANUARY 16, 2001

A comparison of water vapor derived from GPS occultations and global weather analyses

E. R. Kursinski and G. A. Hajj

Jet Propulsion Laboratory, California Institute of Technology, Pasadena

Abstract. Despite its fundamental importance in radiative transfer, atmospheric dynamics, and the hydrological cycle, atmospheric water is inadequately characterized particularly at a global scale. Occultation measurements from the Global Positioning System (GPS) should improve upon this situation. Individual occultations yield profiles of specific humidity accurate to 0.2 to 0.5 g/kg providing sensitive measurements of lower and middle tropospheric water vapor with global coverage in a unique, all-weather, limb-viewing geometry with several hundred meters to a kilometer vertical resolution. We have derived water vapor profiles from June 21 to July 4, 1995, using GPS occultation data combined with global temperature analyses from the European Center for Medium-Range Weather Forecasts (ECMWF) and reanalyses from the National Centers for Environmental Prediction (NCEP). The zonal mean structure of the profiles exhibits basic climatological features of tropospheric moisture. Specific humidity biases between the GPS results and the ECMWF global humidity analyses in the middle to upper troposphere are ~0.1 g/kg or less. Occultation results below 6 km altitude are generally drier than those of ECMWF with the bias generally increasing toward warmer temperatures. Near the height of the trade wind inversion, the ECMWF analyses are significantly moister than the occultation results due to vertical smoothing and overextension of the boundary layer top in the analyses. Overall, the occultation results are drier than the NCEP reanalyses with a marked exception near the Intertropical Convergence Zone (ITCZ) where occultation results are wetter by more than 10%. The occultation results are significantly wetter near the ITCZ and drier in the subtropics than the classical moisture climatology of Peixoto and Oort. Similarities between the NCEP and the Peixoto and Oort near-ITCZ differences suggest that a common analysis/model problem may be responsible. The generally wetter Peixoto and Oort results in the subtropics are due in part to moist radiosonde biases. Discrepancies between these data sets are significant and limit our ability to resolve uncertainties in moisture control and feedbacks in a changing climate.

1. Introduction

Water vapor is a crucial element in weather, climate, and hydrology. It is fundamental to the global energy and hydrological cycles, and the transfer of energy via its phase changes provides much of the energy that drives atmospheric circulation. Moisture availability over land largely defines the continental biosphere, making precipitation and its predictability extremely important. Moreover, water vapor is the dominant greenhouse gas with a nonlinear sensitivity to thermal perturbations resulting from changes in other greenhouse gas concentrations. Even though upper tropospheric concentrations are orders of magnitude less than those in the boundary layer, water vapor distribution throughout the troposphere exerts a large influence on surface temperature [*Shine and Sinha*, 1991]. The small amount of atmospheric moisture in the liquid and solid condensed states exerts an enormous influence on both shortwave and longwave radiative transfer within the atmosphere. The complexity of clouds is such that even the sign of their influence under predicted climatic change scenarios is uncertain. The phase transitions of water are fundamental in transferring energy from the surface into the atmosphere accounting for roughly 3 times the transfer associated with sensible heating [*Kiehl and Trenberth*, 1996].

Paper number 2000JD900421.
0148-0227/01/2000JD900421$09.00

The need for global high vertical resolution observations of water vapor, leading to a better characterization and understanding of the global energy and hydrological cycles, particularly over oceanic regions, has been discussed by *Starr and Melfi* [1991]. Studying Earth's environment at the planetary scale requires precise and globally distributed measurements from space. Present satellite observations of moisture have yielded much insight into the horizontal distribution of water vapor on a global scale. However, the vertical information is limited to an integrated column or a few levels spread across the troposphere, quite coarse in comparison to the scales over which water is known to vary. Furthermore, infrared (IR) soundings are limited by the presence of clouds and aerosols. Passive microwave remote sensing instruments are also subject to biases and ambiguities associated with surface emissivity. These problems limit our ability to characterize the climatological behavior of atmospheric moisture and to analyze and simulate important aspects of the climate system.

A Global Positioning System (GPS) occultation occurs when a GPS satellite is setting or rising behind the Earth's limb as viewed by a receiver in low-Earth orbit. GPS occultation measurements complement passive IR and microwave sounders in several aspects. GPS occultations (1) provide an active probing

of the atmosphere, (2) work under all-weather conditions due to the insensitivity of the ~20 cm GPS wavelength to scattering by clouds, aerosols, and precipitation, (3) provide relatively high vertical resolution throughout the depth of the troposphere associated with the limb-viewing geometry, and (4) provide bias-free estimates of refractivity due to insensitivity to surface emissivity, very accurate measurements of the signal time delay, and the ability to calibrate the source signal during each occultation, making these observations free of any long-term drift. Each GPS occultation yields a profile of refractivity from ~50 km altitude to the surface. By combining the ideal gas law and hydrostatic equilibrium, refractivity profiles can be converted into pressure and temperature profiles in regions where water vapor is negligible in the upper troposphere and middle atmosphere. In the middle and lower troposphere, given an independent knowledge of temperature, GPS refractivity measurements are best used to derive profiles of water vapor partial pressure or specific humidity, complementing passive observations of radiance which are related more directly to relative humidity. The resolution of a GPS occultation is set by the Fresnel diffraction-limited pencil-shaped sampling volume of each measurement which has a horizontal resolution of 200–300 km in the direction along the occulted link and a resolution of the diameter of the first Fresnel zone (~1 km or better) in the cross-link and vertical directions. The ~1 km or better vertical resolution significantly surpasses that obtained from present satellite observations. (For a detailed description of the GPS occultation technique, resolution, and theoretical accuracy, see *Kursinski et al*. [1997].)

Radio occultations have been applied for decades in NASA's planetary occultation experiments [e.g., *Fjeldbo et al*., 1971; *Tyler*, 1987]. However, the application of the technique to sense the Earth's atmosphere had to await the development of an infrastructure built for entirely different purposes, namely, the set of 24 GPS satellites launched and maintained by the Department of Defense (DOD) for the purpose of navigation. As these satellites became operational, it became clear to some [e.g., *Yunck et al*., 1988; *Gurvich and Krasil'nikova*, 1990] that placing a receiver in low-Earth orbit (LEO), with a full 360° field of view of the Earth's limb, would provide about 500 globally distributed occultations daily at a very low cost. This concept was tested for the first time with the GPS Meteorology (GPS MET) experiment which launched a GPS receiver in LEO in April 1995. The GPS-MET experiment, managed by the University Corporation for Atmospheric Research (UCAR) [*Ware et al*., 1996], consisted of a 2 kg GPS receiver piggybacked on the MicroLab I satellite, which has a circular orbit of 740 km altitude and 70° inclination. The GPS receiver is a space-qualified TurboRogue [*Meehan et al*., 1992] capable of tracking up to eight GPS satellites simultaneously at both frequencies transmitted by GPS. Because of the limited field of view of the GPS receiver's antenna and the onboard memory limitation of the satellite, the GPS-MET receiver collected between 100 and 200 globally distributed occultations daily until February 1997.

Several studies have shown that GPS-MET temperature profiles are accurate to better than 1°–2°K between ~5 and 30 km altitudes [*Hajj et al*., 1996; *Kursinski et al*., 1996; *Ware et al*., 1996; *Rocken et al*., 1997] and that geopotential heights of constant pressure levels in the same region are accurate to better than 20 m [*Leroy*, 1997].

Our objectives in this study are (1) to demonstrate the ability to derive tropospheric water vapor profiles from the GPS occultations, (2) to assess the quality of these profiles, and (3) to characterize the present knowledge of water vapor, particularly as represented by global humidity analyses such as those of the European Center for Medium-range Weather Forecasts (ECMWF) and National Centers for Environmental Prediction (NCEP). These objectives are accomplished first by comparing individual water vapor profiles obtained from the GPS MET with those derived from nearby radiosondes and the analyses and, second, by comparing time and zonal averages of water vapor obtained from GPS MET with corresponding averages obtained from the ECMWF analyses, NCEP reanalyses, and the classic moisture climatology developed by *Peixoto and Oort* [1992]. Given the limited GPS-MET data set, zonal averaging is necessary to improve the statistical robustness of the global moisture distribution estimate. Through these comparisons, we also hope to gain some insight into the impact of GPS occultation data on water vapor characterization and modeling.

Our paper is structured as follows: In section 2 we present a summary of how middle and lower tropospheric water vapor profiles can be derived from GPS occultation measurements. Section 3 describes the expected errors in derived specific humidity. Section 4 describes some technical details regarding the processing of GPS/MET data collected during June 21 to July 4, 1995, and how this data set compares with a somewhat inferior data set collected earlier in the experiment. In section 5 we present several individual profiles of water vapor and compare them with the ECMWF analyses and nearby radiosondes. In section 6 the zonal mean distribution of GPS-derived moisture and several associated climatological features are presented. The GPS-based zonal mean humidity is compared with the ECMWF analyses, NCEP reanalyses, and the climatology of Peixoto and Oort in section 7. A summary and conclusions are given in section 8.

2. Deriving Water Vapor Profiles From GPS Occultations

In a GPS radio occultation, the primary observable is the additional propagation delay due to the reduction of the speed of light in the atmosphere relative to a vacuum. The time rate of change of the additional delay is directly related to the bending angle from which the atmospheric index of refraction is derived as a function of height [*Fjeldbo et al*., 1971]. Atmospheric refractivity at microwave wavelengths is given by (*Smith and Weintraub* [1953], see also *Thayer* [1974] and *Kursinski et al*. [1997]).

$$N \equiv (n - 1) \times 10^6 = a_1 \frac{P}{T} + a_2 \frac{P_w}{T^2}, \qquad (1)$$

where

n index of refraction;
P_w partial pressure of water vapor;
P total pressure and is equal to the sum of the dry air pressure P_d and P_w;
T temperature;
a_1 77.6 N-units K mbar^{-1};
a_2 3.73×10^5 N-units K^2 mbar^{-1}.

The first and second terms on the right-hand side of (1) (hereinafter referred to as the hydrostatic and moist terms, respectively) are due to the polarizability of the molecules and the permanent dipole moment of the water vapor molecule, respectively. To solve for P, T, and/or P_w given N, we use the

additional constraints of hydrostatic equilibrium and ideal gas laws given, respectively, as

$$\frac{dP}{dh} = -g\rho, \tag{2}$$

$$\rho = \rho_d + \rho_w = \frac{m_d P}{TR} + \frac{(m_w - m_d) P_w}{TR}, \tag{3}$$

where

h height;
g gravitation acceleration;
ρ, ρ_d, ρ_w total, dry air, and water vapor densities, respectively;
m_d, m_w mean molecular mass of dry gas and water vapor, respectively;
T temperature;
R universal gas constant.

Combining (2) and (3) and using (1) to substitute for P/T, we obtain

$$\frac{dP}{dh} = -\frac{gm_d}{a_1 R} N + \frac{a_2 g m_d}{a_1 R} \frac{P_w}{T^2} + \frac{g(m_d - m_w)}{R} \frac{P_w}{T}. \tag{4}$$

Given N, we have a system of two equations, (1) and (4), and three unknowns (T, P, and P_w). Because saturation vapor pressure decreases exponentially with decreasing temperature, as dictated by the Clausius-Clapeyron equation, and water vapor mixing ratios are parts per million in the middle atmosphere, P_w can essentially be ignored above the tropospheric height corresponding to $T \sim 230$ K; therefore given N, both T and P can be solved for in the upper troposphere and the stratosphere from (1) and (4) and a boundary condition (usually taken to be a temperature boundary condition at ~50 km). However, when P_w is significant, such as in the middle and lower troposphere, it is necessary to have an independent knowledge of one of the three parameters (T, P, P_w) in order to solve for the other two. Given the present knowledge of atmospheric temperature and moisture and their respective variabilities, the information in the refractivity observable primarily constrains P_w in the middle and lower troposphere.

Our approach here is to assume knowledge of $T(h)$ and pressure at some height for a boundary condition, then (1) and (4) are solved iteratively as follows: (1) Assume $P_w(h) = 0$ for a first guess; (2) integrate (4) to obtain $P(h)$; (3) use $P(h)$ and $T(h)$ in (1) to update $P_w(h)$; and (4) repeat steps 2 and 3 until convergence.

Relative humidity U is computed as the ratio of P_w to the saturation vapor pressure P_w^* under the same temperature and pressure conditions. Throughout this paper, saturation is defined over liquid water unless stated otherwise. The moisture variable we discuss most frequently is specific humidity q, which is the mass mixing ratio of water vapor in air. Given P and P_w, q is given by

$$q = \left[\frac{m_d}{m_w} \left(\frac{P}{P_w} - 1 \right) + 1 \right]^{-1}. \tag{5}$$

3. Estimated Accuracy

The relation between errors in N, T, P, and P_w is a function of latitude and height and is described in detail by *Kursinski et al.* [1995]. Here we extend that discussion to characterize errors in specific humidity. The sensitivity of water vapor partial pressure to errors in pressure, temperature, and retrieved refractivity can be assessed by differentiating and manipulating (1) to yield

$$\frac{dP_w}{P_w} = (B + 1) \frac{dN}{N} + (B + 2) \frac{dT}{T} - B \frac{dP}{P}, \tag{6}$$

where B is equal to $a_1 TP/a_2 P_w$ and $a_1 Tm_w/a_2 m_d q$. Since B varies inversely with q, it varies dramatically, particularly in the tropics where it ranges from ~3 near the surface to $\sim 10^4$ near the tropopause. Clearly, the fractional accuracy of water vapor profiles, derived from measurements of microwave refractivity, depends strongly on specific humidity. We can modify (6) to express the accuracy of derived specific humidity

$$\frac{dq}{q} = (B + 1) \frac{dN}{N} + (B + 2) \frac{dT}{T} - (B + 1) \frac{dP}{P}. \tag{7}$$

Defining C as $a_1 Tm_w/a_2 m_d$, changes in q are related to changes in N, T, and P as

$$dq = (C + q) \frac{dN}{N} + (C + 2q) \frac{dT}{T} - (C + q) \frac{dP}{P}. \tag{8}$$

Following the argument of *Kursinski et al.* [1995], we assume the errors in N, T, and the surface pressure P_s are independent such that we can write the approximate error in q as

$$\sigma_q = \left[(C + q)^2 \left(\frac{\sigma_N}{N} \right)^2 + (C + 2q)^2 \left(\frac{\sigma_T}{T} \right)^2 + (C + q)^2 \left(\frac{\sigma_{P_s}}{P_s} \right)^2 \right]^{1/2}. \tag{9}$$

Kursinski et al. [1995, 1997] estimated the errors in refractivity profiles derived from GPS occultation using the Abel transform. Kursinski et al. found that below roughly 30 km altitude the dominant refractivity errors were associated with nonspherical structure not accounted for by the Abel transform. The root-mean-square (rms) errors were ~0.2% above 7 km altitude and grew approximately linearly to ~1% near the surface because the increasing water vapor concentrations at lower altitudes caused greater horizontal refractivity variations via (1). Figure 1 shows the results of (9) for annual mean conditions from *Peixoto and Oort* [1992] using the refractivity error versus height estimated by *Kursinski et al.* [1995] and assuming a temperature error of 1.5 K and surface pressure

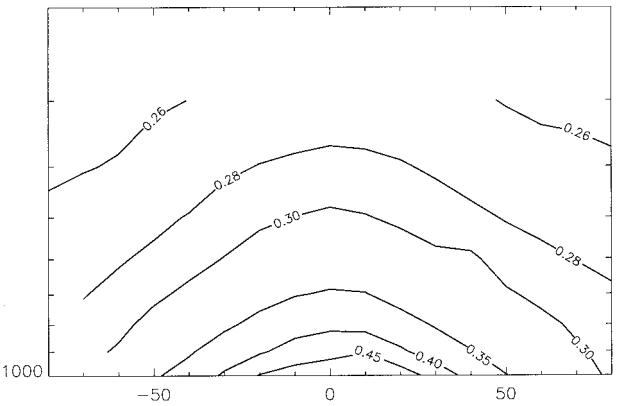

Figure 1. Estimated error in specific humidity profiles derived from GPS refractivity profiles as a function of latitude and altitude for annual mean conditions in g/kg.

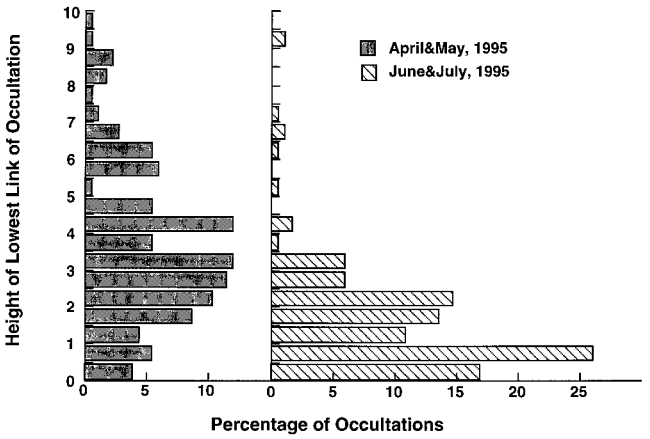

Figure 2. Comparison of histograms of the minimum altitude of occultation profiles for two periods of the GPS-MET mission. (left) Data from April 24 and 25 and May 4 and 5, 1995. (right) Data from June 21, 22, 23, and 27, 1995. Occultations during the second period probed systematically deeper into the atmosphere because of GPS-MET receiver software uploaded during this period modified to significantly improve signal tracking in the troposphere (see text for details).

error of 3 mbar. The error in q ranges from 0.2 to 0.5 g/kg. It is dominated by the temperature error at higher altitudes, whereas the refractivity error becomes the larger contributor near the surface. The relatively small variation in the q error is because C changes by relatively little varying from 32 g/kg at 230 K to 39 g/kg at 300 K, and q varies from ~0 to roughly $C/2$. As a result, the factors multiplying the errors in N, T, and P_s vary by about a factor of 2 over the atmosphere.

Figure 1 and (9) represent the error in individual profiles of specific humidity. Accuracies of averaged specific humidity will be better and will probably be limited by the mean temperature error [*Kursinski et al*., 1995]. Assuming a mean temperature error of 0.5 K, the mean specific humidity error will be roughly 0.1 g/kg.

4. Data Processing Strategy

In this paper we derive refractivity profiles from raw GPS-MET occultation observations and then derive specific and relative humidity, primarily in the middle and lower troposphere, using independent temperature information from the nearest 6 hour ECMWF analysis and NCEP reanalysis, interpolated to the location of each occultation. Our estimates of water vapor and their zonal means are then compared to those derived from the ECMWF analyses and NCEP reanalyses. We concentrate on the period June 21 through July 4, 1995 (excluding June 24–26 because of instrumental problems) for the following reasons:

1. The June–July 1995 (JJ95) period is one of four 2–3 week periods during the GPS-MET mission when the GPS Antispoofing (AS) encryption was turned off to increase the signal to noise ratio (SNR) of the L2 signal as received by the prototype GPS-MET receiver. The L2 signal is used to calibrate and remove the effect of the ionosphere [*Vorob'ev and Krasil'nikova*, 1994]. Beginning in 2000, a series of second generation of occultation receivers developed at the Jet Propulsion Laboratory (JPL) will be placed in LEO and achieve high L2 SNR with the AS encryption on.

2. Modifications to the GPS-MET receiver software made at JPL for the JJ95 period allowed signal tracking through outages as long as 5 s and significantly extended the depth of occultation profiles in the troposphere. As a result, nearly all profiles extend to below 3 km altitude and a large fraction extend to within 1 km of the surface. The impact of this software modification is reflected in the distribution of the lowest height of the occultations acquired in the April–May 1995 period versus the JJ95 period shown in Figure 2.

3. Climatologically, the JJ95 is a good period for assessing GPS occultation water vapor retrievals because June-July-August are characteristic of high specific humidity in the Northern Hemisphere where more measurements and therefore better ground truth exist. Moreover, the zonally averaged tropical Hadley circulation is best defined during this period of the year because the Intertropical Convergence Zone (ITCZ) is north of the equator at most longitudes [*Waliser and Gautier*, 1993].

The ECMWF and NCEP global analyses provide global coverage and high accuracy (as demonstrated by the temperature comparisons in the middle and upper troposphere and stratosphere [*Kursinski et al*., 1996]), with updates every 6 hours. The ECMWF analyses provide high spatial resolution reconstruction of the global atmosphere with 31 vertical levels to 10 mbar and ~100 km horizontal grid spacing. The NCEP reanalyses provide slightly lower resolution with 26 vertical levels to 10 mbar and ~200 km horizontal grid spacing. These resolutions are similar to that of the GPS observations [*Kursinski et al*., 1997].

For each occultation, a profile of refractivity is derived. Starting with a boundary condition of temperature at 50 km altitude and ignoring P_w (in practice, we assume a climatologically representative mixing ratio of several ppm in the middle atmosphere to minimize any systematic bias), P is obtained by integrating (4) down to a tropospheric height where retrieved $T = 230$ K. We refer to this height and the corresponding pressure there by $h_{T=230}$ and $P_{T=230}$, respectively. Equation (1) is then used to derive T. Below $h_{T=230}$, we use the ECMWF or NCEP temperature combined with $P_{T=230}$ as a boundary condition to derive $P_w(h)$ below $h_{T=230}$, using the iterative process described in section 2.

A screening process is applied to the retrieved water vapor on the basis of three basic criteria: (1) Profiles containing jagged, unphysical vertical structure associated with receiver tracking problems were rejected. (2) Water vapor abundance had to be at least crudely reasonable climatologically. (3) Humidities at low altitudes were required to be positive. Out of ~1000 occultations processed at JPL over the JJ95 period, approximately 800 occultations passed the selection criteria.

Profiles with negative humidities at low altitudes were rejected, in general, because low-altitude humidities are typically large such that negative values indicate large nonrandom errors. Such large humidity errors were caused by receiver tracking problems resulting in refractivity profiles well outside the realm of physical possibility. In the subtropical free troposphere, where specific humidities can be very small, we made an exception and did allow profiles with small negative humidities if the refractivity profile appeared reasonable. These cases are discussed in more detail in section 7.8.

At high altitudes, where specific humidities are always small, small random errors can cause small negative specific humidities. For example, an rms temperature error of 1.5 K, which is representative of analysis temperature errors, will cause a 0.2

g/kg rms error in specific humidity. As a result, in a region where the mean specific humidity is 0.1 g/kg, many profiles will include specific humidities of ~ -0.1 g/kg. In averaging these specific humidity profiles, the random errors will average out and the accuracy of the estimated mean will be limited by biases in the analysis temperature and occultation refractivity. Because eliminating profiles with negative values would substantially and erroneously raise the estimate of the mean, we chose to include profiles with small, negative specific humidities at high altitudes to improve our estimate of mean humidity.

For this initial examination of water vapor we have chosen the simple approach of using the ECMWF analysis and NCEP reanalysis temperatures without adjustment. While the analysis temperatures could be modified to yield only positive and subsaturated specific humidities near the 230 K level, these modifications may alter atmospheric stability in undesirable and dynamically inconsistent ways. Changing the temperature profile in a self-consistent manner is beyond the scope of the present effort and will be addressed in the future.

5. Individual Profile Examples

In this section we discuss three representative GPS-MET water vapor profiles to illustrate the resolution of the occultation retrievals and the differences between the occultations, ECMWF analyses, and radiosondes.

Figure 3 shows a specific humidity profile derived from GPS/MET together with profiles from interpolated ECMWF analysis and three nearby radiosondes a few hundred kilometers northeast of Helsinki, Finland. With the exception of the southwestern sonde profile below 6 km altitude, the profiles generally agree. The southwestern sonde profile is distinctly drier than the other profiles below 6 km altitude with a sharply defined isohumid region extending from 4 to 5.5 km altitude. Note that the isohumid region in the GPS-MET profile coincides roughly in altitude with that of the southwestern radiosonde but is not present in the moisture profile of the ECMWF analysis. The ECMWF analysis temperature used to derive the GPS-MET specific humidity profile (top curve in Figure 3) exhibits no corresponding structure, indicating that the isohumid structure in the GPS-MET profile comes entirely from the retrieved refractivity structure. The sharpness of the resolved isohumid region indicates vertical resolution of the occultation data consistent with the 200–1000 m resolution expected of in the troposphere [*Kursinski et al*., 1997]. In contrast, the vertical structure of the ECMWF analysis moisture profile is quite smooth above 1.5 km altitude. Overall, the GPS-MET profile appears as a combination of the two smoother profiles to the east and the drier, more variable profile to the southwest.

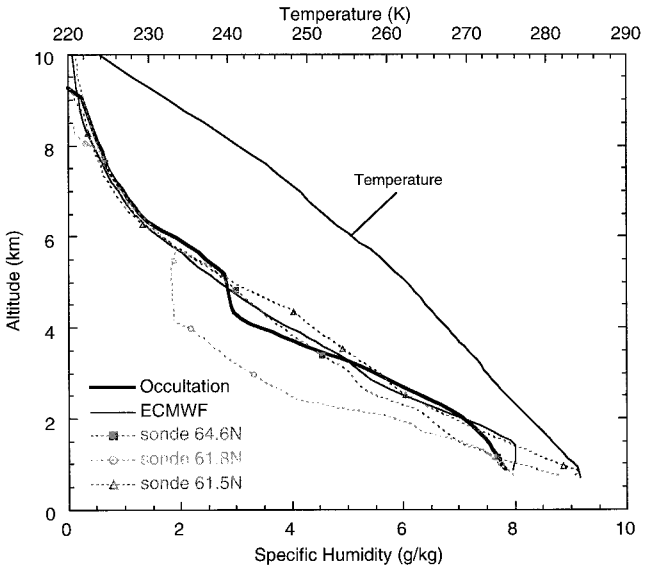

Figure 3. Comparison of five specific humidity profiles northeast of Helsinki from June 22, 1995. The five profiles are humidity derived from a GPS refractivity profile at 0349 UT located at 63.15°N, 36°E (thick solid line), humidity from the global ECMWF analysis at 0600 UT interpolated to the occultation location (line with solid squares) and three nearby radiosondes taken at 0000 UT (thin solid line, sonde at 64.6°N, 40.5°E; line with circles, sonde at 61.8°N, 34.3°E; line with inverted triangles, sonde at 61.5°N, 38.9°E). Also shown on the upper scale is the ECMWF temperature profile interpolated to the occultation location used to convert refractivity to specific humidity. Note that since the temperature profile is quite smooth, the vertical variations in the GPS-derived water vapor profile particularly that of the isohumid structure between 4 and 5 km altitude comes entirely from the GPS refractivity information.

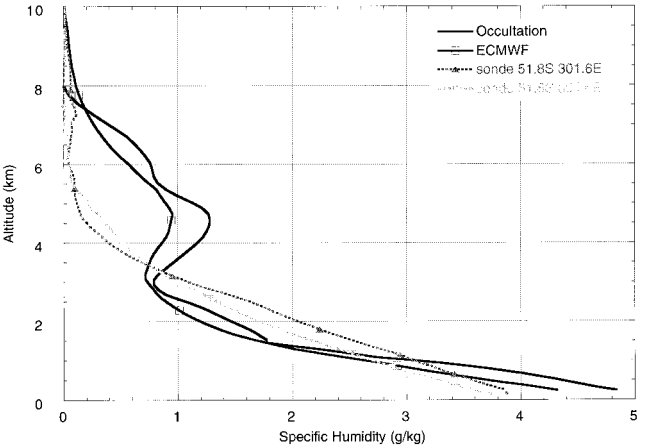

Figure 4. Comparison of four specific humidity profiles from June 23, 1995, in the southern Atlantic Ocean northeast of the Falkland Islands. The occultation occurred at 0407 UT at 49.4°S, 302.9°E and is indicated with the solid line with cross hatches. The interpolated ECMWF humidity analysis profile is the solid line. The two sondes launched from the Falkland Islands at 51.8°, 301.6°E are indicated by triangles (0000 UT) and inverted triangles (0600 UT).

Figure 4 shows a GPS-MET humidity profile roughly 300 km northeast of the radiosonde site on the Falkland Islands. The occultation and ECMWF analysis humidity profiles both exhibit a relative maximum in specific humidity near 4.5 km altitude. In contrast, the two radiosonde profiles separated by 6 hours exhibit a smooth, approximately exponential decay of moisture with height. The explanation for the differences is that the occultation and radiosondes are sampling distinctly different air masses with the occultation falling within an occluded front lying to the northeast of the Falklands (A. Hollingsworth, personal communication, 1997). The consistency between the GPS-MET and ECMWF analysis profiles demonstrates the ability of the analysis to determine an elevated relative maximum in specific humidity in a remote area reflecting the impact of the TIROS Operational Vertical Sounder

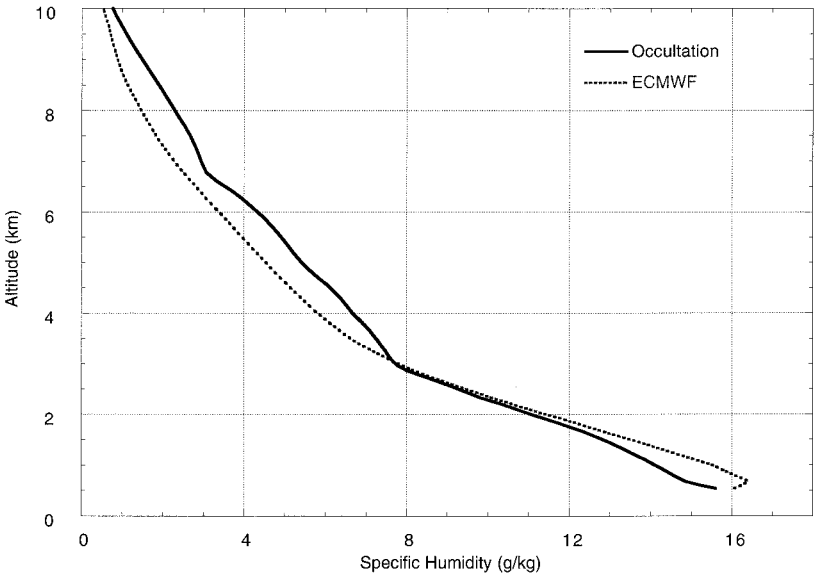

Figure 5. Comparison of specific humidity profiles from June 27, 1995, near Sri Lanka. The two profiles shown are derived from an occultation at 0531 UT located at 6.3°S, 88.8°E (solid line) and ECMWF humidity analysis at 0600 UT interpolated to the occultation location (dotted line). Of note is the ability of the occultation to retrieve moisture structure to the surface under very moist conditions.

(TOVS) data on the global analyses. A final point is that the occultation profile extends to the surface.

Figure 5 shows a low-latitude profile southeast of Sri Lanka together with the interpolated analysis profile demonstrating the ability to derive moisture down to near the surface under some of the wettest conditions on Earth. Vertical variations in moisture when specific humidities are high can cause dramatic variations in signal intensity and multiple images of the signal to be present at the receiver causing tracking problems [*Kursinski et al.*, 1997]. In the present example the prototype GPS receiver was able to track the occulted signal to the surface because the moisture increases relatively smoothly at lower altitudes as indicated by both the GPS-MET and the ECMWF analysis humidity profiles. With GPS receiver improvements under development at JPL, we anticipate that most occultation profiles will extend to the surface.

6. Zonal Mean Specific and Relative Humidity Structure

6.1. GPS-MET Coverage for June 21 to July 4, 1995, Period

The latitude-longitude distribution of the occultation data acquired by GPS MET during the JJ95 period is given in Figure 6 (top). Although 250 occultations per day are potentially available from an orbiting GPS receiver with a single antenna (facing forward or backward), the total number of daily occultations available from GPS MET is roughly 100 per day due to memory and telemetry downlink constraints. The sampling, while somewhat sparse, probably offers the best available combination of global coverage and vertical resolution. To estimate the zonal means, data were binned every 250 m in altitude and every 5° of latitude with a bin width of 250 m and 10° of latitude. The resulting sampling density of the 800 occultations in the height-latitude bins is shown in Figure 6b.

6.2. Sampling Adequacy and Zonal Approach

Before discussing the GPS zonal mean results, it is useful to characterize the adequacy of the 800 occultations for capturing zonal mean behavior for the JJ95 period. We can do so by estimating the zonal mean behavior from a set of 800 "profiles" derived from the 6 hour global ECMWF analyses interpolated to the 800 occultation locations (which we refer to as IE) and comparing this estimate with the zonal mean derived from the complete set of ECMWF analyses for the JJ95 period (referred to as CE) where the averaging is over four analyses per day and 10 days. We make the IE versus CE comparison in terms of both temperature and specific humidity. In the remaining part of this paper the following notation is used:

q_{GE} and U_{GE} specific and relative humidity, respectively, derived from GPS occultation refractivity with temperature given by the ECMWF analyses;

q_{GN} and U_{GN} specific and relative humidity, respectively, derived from GPS occultation refractivity with temperature given by the NCEP reanalyses;

q_G and U_G averages of q_{GE} and q_{GN} and U_{GE} and U_{GN}, respectively;

q_{CE} and U_{CE} zonal mean of specific and relative humidity, respectively, obtained from the complete set of the ECMWF analyses during JJ95;

q_{IE} and U_{IE} zonal mean of specific and relative humidity, respectively, obtained from the interpolated set of the ECMWF analyses during JJ95;

q_{IN} and U_{IN} zonal mean of specific and relative humidity, respectively, obtained from the

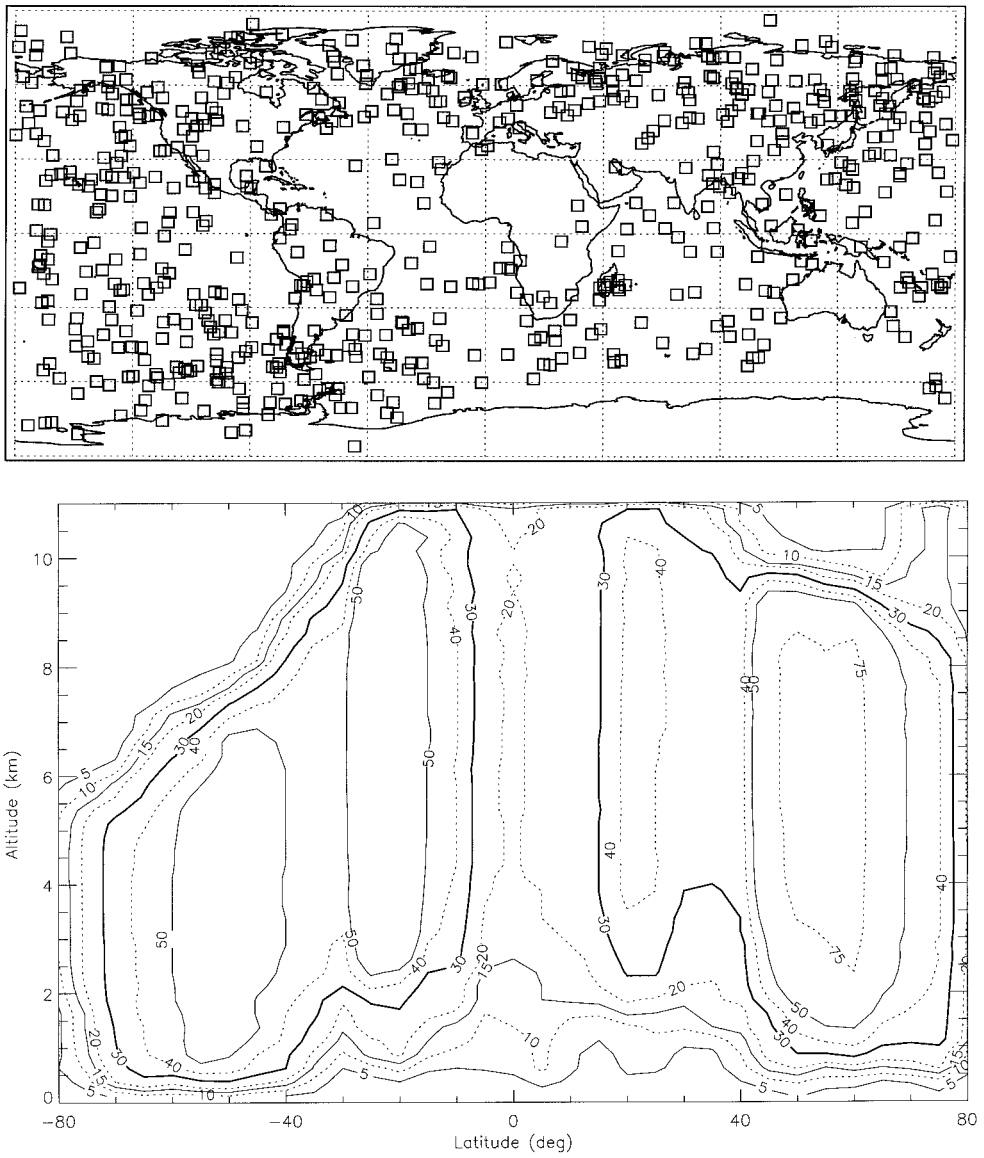

Figure 6. Spatial distribution of the 800 occultations in the JJ95 period. (top) The distribution of the occultations versus latitude and longitude. (bottom) Contour plot of the latitude versus height distribution of the occultations in terms of the number of occultations per latitude-height bin. Bins are 250 m high and 10° of latitude wide. Averages calculated in each bin are the estimates of the zonal mean structure.

interpolated set of the NCEP reanalyses during JJ95;

q_{PO} zonal mean of specific humidity based on the June, July, and August (JJA) climatology of *Peixoto and Oort* [1992];

q_A average of q_G, q_{IE}, and q_{IN}.

Overbars refer to the zonal means of these quantities.

Figures 7 (top) and 7 (bottom) show the zonal mean temperature estimates derived from the CE and IE data sets. The similarity between the figures indicates that the IE data set is representative of the climatological conditions of the JJ95 period. In the region between 20°S and 30°N the warmest temperatures and smallest meridional gradients are found. Temperature values are distinctly lower and meridional temperature gradients larger in the Southern Hemisphere than in the Northern Hemisphere indicative of the seasonal contrast between the hemispheres and the baroclinicity driving the large winter storms. The largest discrepancy between the IE and the CE results occurs over Antarctica where the IE temperatures are some 2–5 K warmer than those of CE, indicating the JJ95 occultation sample set is not entirely representative of conditions there.

Figures 8 (top) and 8 (bottom) show the zonal mean specific humidity estimates from the CE and IE data, respectively, for the JJ95 period. The comparison reveals some discrepancies such as the weak relative maximum in $\bar{q}_{IE}$ south of 70°S over Antarctica which is not present in $\bar{q}_{CE}$, a relative maximum near 30°N in the free troposphere which is more meridionally distinct in $\bar{q}_{CE}$ than in $\bar{q}_{IE}$, and the sharp meridional gradient in $\bar{q}_{IE}$ near 45°N above 4 km altitude is smoother in $\bar{q}_{CE}$. Results within 1 km of the surface in the Northern Hemisphere are also somewhat noisy due to the limited number of occul-

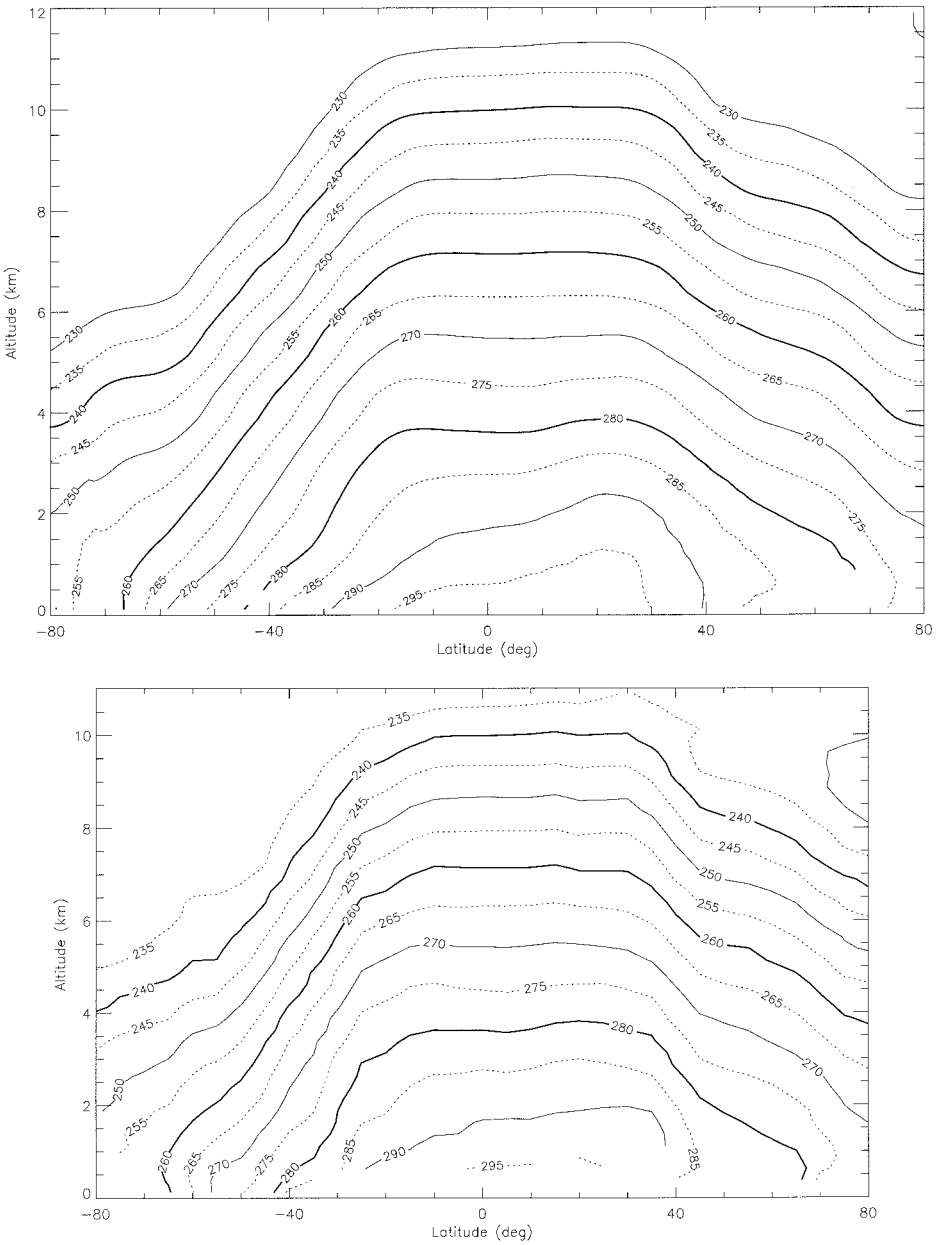

Figure 7. Zonal mean temperatures for the JJ95 period. (top) The zonal mean temperature derived from the complete set of ECMWF analyses (CE). (bottom) Zonal mean of 800 profiles derived from the 6 hour global ECMWF analyses (IE) to coincide with the occultation locations.

tation profiles reaching this altitude interval (Figure 6 (bottom)). While some discrepancies do exist because of the limited sampling of the occultations, the IE and CE estimates are generally consistent, indicating that the occultation sampling adequately captures the mean zonal behavior for the period in general.

6.3. Random Errors in GPS Moisture Estimates

Random errors in the specific humidity profiles derived from GPS refractivity profiles have been discussed in section 3. Upon averaging multiple profiles to estimate zonal mean moisture, the random error contribution to the mean will decrease by the square root of the number of averaged profiles. The resulting random error contribution to the zonal mean specific humidity, based on the occultation sampling density in Figure 6 (bottom), is shown in Figure 9. In general, the random error contribution is small in comparison to the zonal mean specific humidity estimates in Figure 8.

6.4. Impact of Temperature Biases on GPS Moisture Estimates

Because we rely on the analysis temperatures to isolate the water vapor contribution to the retrieved refractivity profiles, any systematic analysis temperature errors also contribute to errors in the GPS humidity estimates. The magnitude of this error is reflected in the differences between $\bar{q}_{\mathrm{GE}}$ and $\bar{q}_{\mathrm{GN}}$ (Figure 10 (top)), which are due only to differences between the analyzed ECMWF and NCEP temperatures. Specific humidity differences are generally 0.1 g/kg or less. Agreement is best in the Northern Hemisphere. In fractional terms (Figure

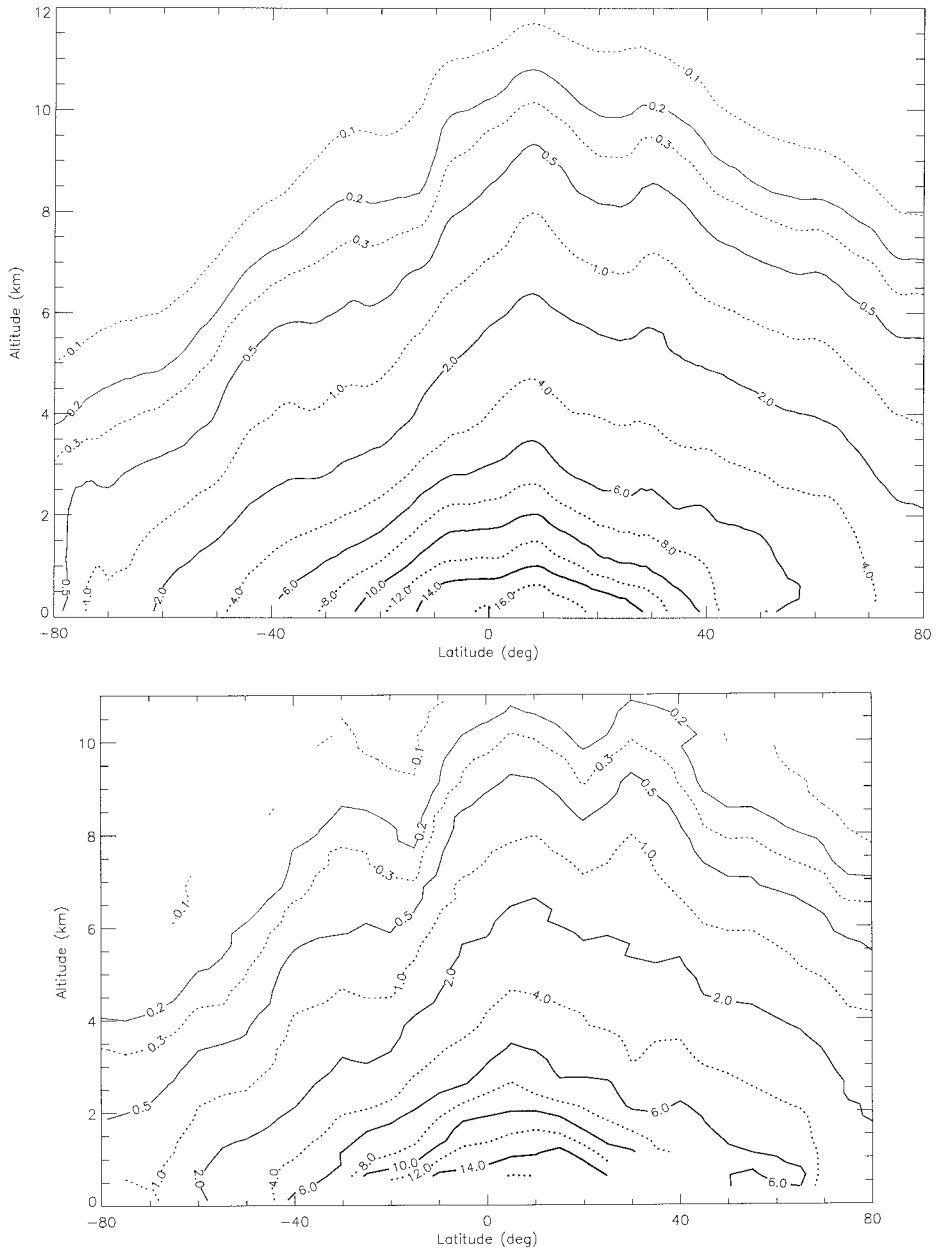

Figure 8. Two estimates of zonal mean specific humidity. (top) $\bar{q}_{\mathrm{CE}}$ for JJ95. (bottom) $\bar{q}_{\mathrm{IE}}$ for JJ95. Contours are at 0, 0.1, 0.2, 0.3, 0.5, 1, 2, 4, 6, 8, 10, 12, 14, and 16 g/kg.

10 (bottom)), agreement is best in the Northern Hemisphere and lower regions of the low latitudes with fractional humidity differences smaller than 10%. In the upper troposphere near 20°S, humidity estimated using ECMWF temperatures is lower by more than 20% in specific humidity because ECMWF temperatures are lower than NCEP temperatures by ~0.5 K. Discrepancies increase toward southern high latitudes and high altitudes, which reflects both the low specific humidities there and the generally less accurate analyzed temperatures there during the JJ95 period. The largest differences occur near 3 km altitude at 80°S where $\bar{q}_{\mathrm{GN}}$ becomes negative because NCEP analysis temperatures are too cold by ~2 K. We also note that since only $\bar{q}_{\mathrm{GE}}$ exhibits a sharp zonal oscillation between 50°S and 75°S, whereas the other three zonal moisture estimates, $\bar{q}_{\mathrm{IE}}$, $\bar{q}_{\mathrm{IN}}$, and $\bar{q}_{\mathrm{GN}}$, do not, it is likely that the subset of ECMWF temperatures interpolated to the times and locations of the occultation profiles in the 50°S–75°S zone have erroneous meridional temperature variations of the order of 1 K.

Given the differences between $\bar{q}_{\mathrm{GE}}$ and $\bar{q}_{\mathrm{GN}}$, and the uncertainties in determining which set of temperature analyses is better (given that each appears to have its own set of limitations), we have chosen to take the average of $\bar{q}_{\mathrm{GE}}$ and $\bar{q}_{\mathrm{GN}}$ as the GPS moisture estimate for the remainder of this paper. By taking the average we hope to reduce the magnitude of any extreme errors by a factor of 2. We will refer to this average GPS specific humidity estimate as $\bar{q}_{\mathrm{G}}$ (Figure 11) and the corresponding relative humidity estimate as $\bar{U}_{\mathrm{G}}$ (Figure 12). We also form the average of $\bar{q}_{\mathrm{G}}$, $\bar{q}_{\mathrm{IE}}$, and $\bar{q}_{\mathrm{IN}}$ (referred to as $\bar{q}_{\mathrm{A}}$ (Figure 13)) against which all fractional specific humidity differences are normalized.

Figures 9 and 10 are consistent with the expectation derived in section 3 that zonal mean moisture can be derived from GPS

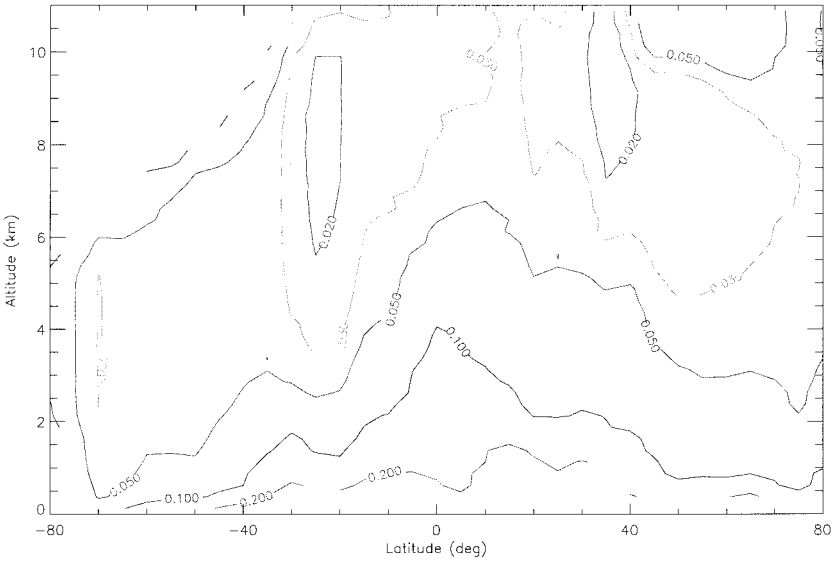

Figure 9. Estimated zonal mean specific humidity error due to random errors in moisture profiles derived from GPS refractivity profiles and analysis temperatures.

occultations to ~0.1 g/kg accuracy. Therefore differences between GPS estimates of zonal mean humidity and ECMWF and NCEP moisture analyses whose magnitudes are significantly larger than the values in Figures 9 and 10 can be attributed to systematic moisture differences or biases between the GPS retrievals and the moisture analyses. These differences are discussed further below.

6.5. Zonal Mean Humidity Derived From GPS/MET Results

The GPS zonal mean specific humidity $\bar{q}_G$ in Figure 11 exhibits several basic climatological features. (1) Specific humidity decreases dramatically with altitude. (2) Values of $\bar{q}_G$ in the Northern (summer) Hemisphere are larger than their Southern (winter) Hemisphere counterparts by factors of 2–4. The larger meridional gradient in the Southern Hemisphere is qualitatively consistent with the larger meridional temperature gradients in the winter hemisphere. (3) The mean specific humidity has a well-defined peak centered near 5°N to 10°N, the approximate location of the Intertropical Convergence Zone (ITCZ). (4) Maximum $\bar{q}_G$ values of 14 g/kg are found near the ITCZ between 0.5 and 1 km altitude; still higher mean values would be visible presumably if the profiles extended to the surface in this zone. (5) A large meridional gradient in $\bar{q}_G$ exists near 15°S, which is associated with the transition between the upwelling regions and the southern subsiding branch of the tropical Hadley circulation. (6) A peak in $\bar{q}_G$ exists near 30°N between 8 and 11 km altitude, which is associated with the injection of moisture into the middle and upper troposphere by the Asian/Indian summer monsoons. (7) There is also a smaller peak near 30°S above 2 km altitude which appears to be associated with the transition between the subtropical zone of subsidence and the winter baroclinic region.

Figure 12 shows the zonal mean relative humidity, $\bar{U}_G$, estimated from the GPS data. It is important to note that the GPS observations are closely related to specific humidity because refractivity essentially represents a molecule counter. Occultation observations are not directly sensitive to relative humidity in contrast to radiance observations, which are more directly related to relative humidity [*Soden and Bretherton*, 1996]. One can, of course, derive individual profiles of relative humidity (U_G) as the ratio of GPS-derived water vapor pressure to saturation pressure at the interpolated analysis temperature, and $\bar{U}_G$ would be estimated by averaging these profiles. However, the sensitivity of this ratio to temperature errors when specific humidities are small causes the relative humidities to be noisy and biased low (see Appendix). As a result, near 60°S above 5 km altitude, the zonal mean relative humidity estimate is negative, while the mean specific humidity estimate is positive. This odd situation is because we have consciously allowed profiles with small negative humidities at upper altitudes in order to derive an accurate estimate of the mean specific humidity (section 4) and because the ECMWF temperature errors are unusually large in this region with an rms error ~2.6 K (see Appendix). The conclusion that temperature errors in this region are large is consistent with the results of *Kursinski and Hajj* [2000] who characterized the meridional dependence of the ECMWF temperature errors further.

To reduce the dry bias in the GPS relative humidity results caused by temperature errors, we have chosen to represent $\bar{U}_G$ as the ratio of mean partial pressure of water vapor to the saturated partial pressure of water vapor at the zonal mean temperature of the ECMWF and NCEP analyses. The zonal mean relative humidity estimate derived this manner ($= \bar{U}_G$), shown in Figure 12, reflects several basic climatological features. (1) The relative maximum in $\bar{U}_G$ between 0° and 10°N coincides approximately with the ITCZ, the zone of upwelling in the tropical Hadley circulation. (2) A relative minimum exists to either side of the ITCZ which coincides with the zones of subtropical subsidence. (3) The asymmetry of the tropical Hadley circulation is evident with minimum $\bar{U}_G$ values of 10–20% between 10°S and 30°S (corresponding to a global minimum of $\bar{U}_G$) versus minimum $\bar{U}_G$ values of ~30% in the northern subsidence zone. The asymmetry of the zonal mean relative humidity about the ITCZ reflects the asymmetry of the tropical Hadley circulation during northern summer. In the northern summer the rising branch of the tropical Hadley

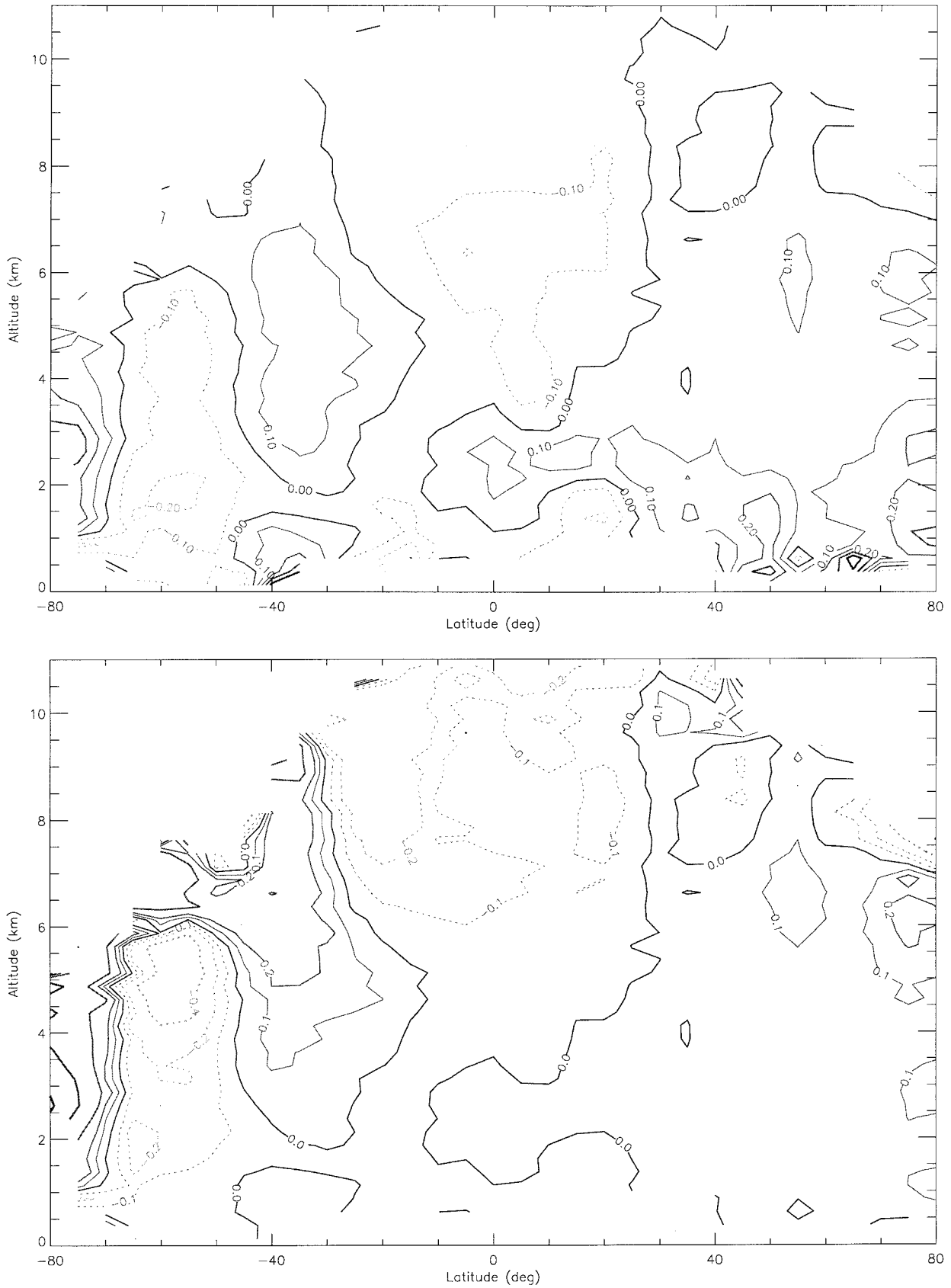

Figure 10. Zonal mean differences between the GPS specific humidity profiles derived using temperatures from the ECMWF analyses and the NCEP reanalyses ($\bar{q}_{GE} - \bar{q}_{NE}$) for JJ95. (top) Specific humidity differences in g/kg. Contours are at 0, +0.1, +0.2, +0.4, +1, and +2 g/kg. (bottom) Fractional specific humidity differences. Contours are at 0, +0.1, +0.2, +0.4, +1.

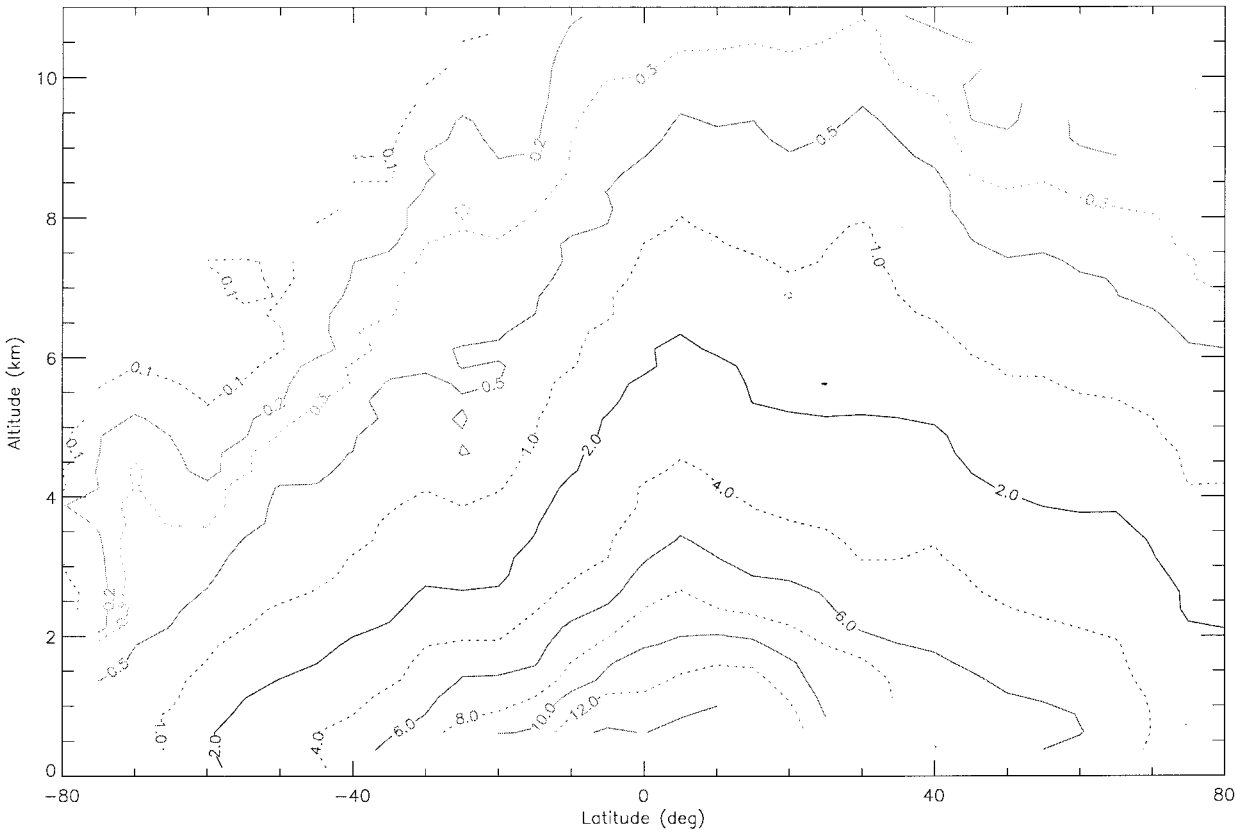

Figure 11. Zonal mean specific humidity derived from the GPS refractivity estimates for JJ95 as represented by the average of $\bar{q}_{\mathrm{GE}}$ and $\bar{q}_{\mathrm{GN}}$ in g/kg.

circulation is generally in the summer hemisphere, the stronger subsiding branch is in the winter hemisphere, and the weaker subsiding branch is in the summer hemisphere [*Peixoto and Oort*, 1992]. (4) High relative humidities near the surface and the general decrease at higher altitudes reflect the surface source of tropospheric moisture.

7. Comparisons With Global Moisture Analyses

In this section we compare the zonal mean specific humidities for the JJ95 period derived from GPS occultation refractivity profiles ($\bar{q}_{\mathrm{G}}$) with those derived from the ECMWF analyses and NCEP reanalyses interpolated to the occultation times and locations ($\bar{q}_{\mathrm{IE}}$ and $\bar{q}_{\mathrm{IN}}$, respectively). We also compare these results with the classical moisture climatology for June, July, and August (JJA) of *Peixoto and Oort* [1992] (hereinafter PO). Our goal is to identify and quantify systematic biases between the GPS retrievals and the other three analyses and, to the extent possible, identify their sources.

7.1. Analysis Characteristics

The GPS moisture estimate characteristics and errors have been discussed in sections 3 and 6. The ECMWF analyses represent the global atmosphere derived from a combination of a model and satellite and radiosonde data. During the JJ95 period the data included TOVS satellite data which provide daily global coverage and radiosonde profiles where and when available. The TOVS radiances were assimilated into the ECMWF analyses in a one-dimensional (1-D) Var scheme after December 1994. The TOVS moisture data consist primarily of radiance measurements from three IR channels at 6.7, 7.3, and 8.3 μ which are sensitive to the humidity integrated over layers centered in the upper (200–500 mbar), middle (300–700 mbar), and lower troposphere (600 mbar to surface) [*Soden and Bretherton*, 1996]. These broad vertical layers provide some vertical information about moisture distribution in remote regions, as noted in Figure 4. Interpretation of the TOVS radiances in terms of moisture is nonunique, and the vertical contribution function depends on the amount of moisture present. Assimilation of TOVS data also makes the analyses subject to problems associated with IR observations under cloudy conditions [*Eyre et al*., 1993; *McNally and Vesperini*, 1996]. Other sources of error include the model's physical representation of the hydrological cycle and its inherent resolution.

The NCEP reanalyses are broadly similar to the ECMWF analyses providing the global state of the atmosphere on the basis of a combination of a model and satellite and radiosonde data. Regarding moisture accuracy, *Kalnay et al*. [1996] indicate that the NCEP moisture analyses are a "class B" variable complete with the caveat that "although there are observational data that directly affect the value of the variable, the model also has a very strong influence on the analysis value." Therefore the NCEP moisture reanalyses will reflect model biases.

The PO climatology is based primarily on a network of 1093 radiosonde stations for the period from May 1963 to April 1973 which have been supplemented by daily surface ship reports. The climatology is limited by the extremely sparse and uneven coverage by radiosondes at low and southerly latitudes. Because the PO data were not acquired during JJ95, the

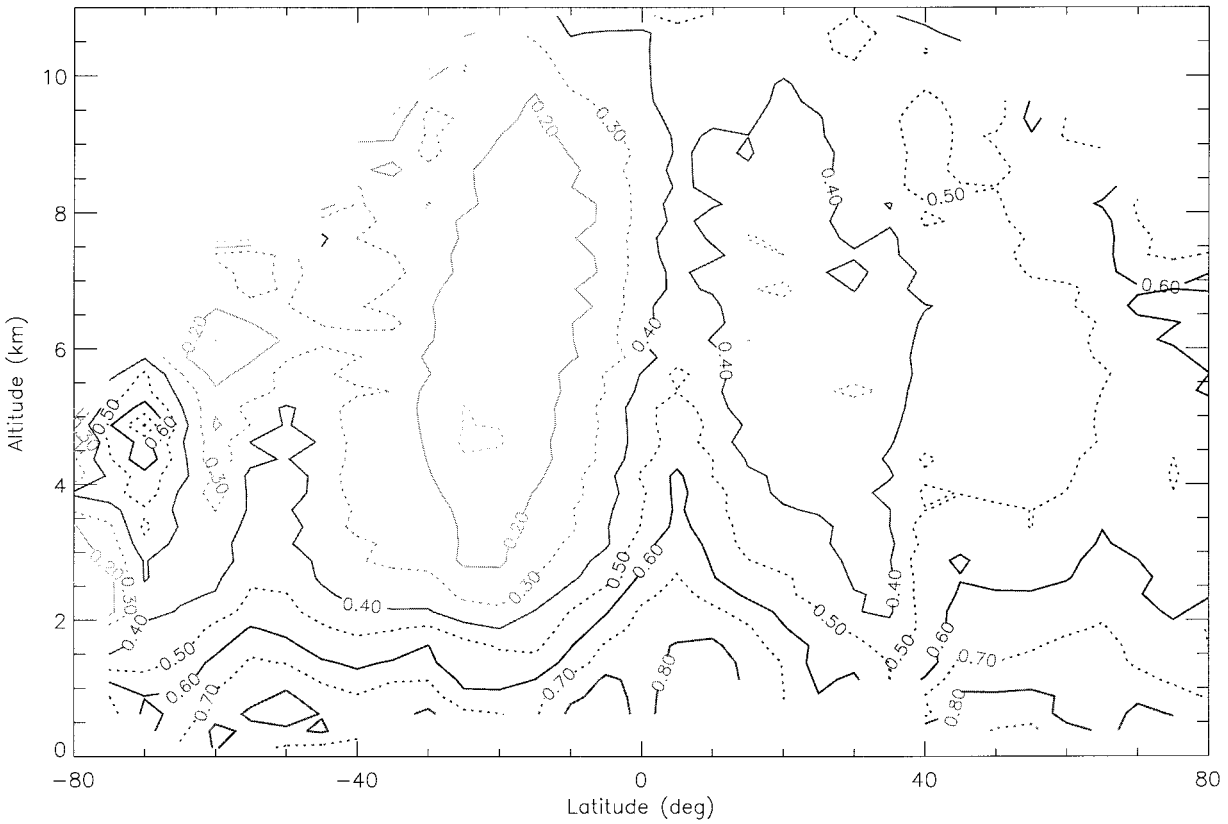

Figure 12. Zonal mean relative humidity derived from the GPS refractivity estimates for JJ95 as represented by the average of $\bar{U}_{GE}$ and $\bar{U}_{GN}$. Contours are separated by 0.1 (= 10% relative humidity). Saturation is defined over liquid water.

GPS-PO differences may have significant contributions from interannual variability or long-term trends.

To gain some insight into present uncertainties in the global moisture distribution, the specific and relative humidity differences between the interpolated ECMWF analyses and the NCEP reanalyses are shown in Figure 14. ECMWF moisture estimates tend to be higher than those of NCEP in regions where the zonal mean specific humidity is greater than 2 g/kg. The low altitude tropical difference is quite large reaching more than 2 g/kg and 10–20% in terms of relative humidity. In regions of low specific humidity the ECMWF specific and relative humidity estimates are generally lower than those of NCEP. The zonal mean differences are greater than 20% relative humidity through large regions of the Southern Hemisphere and upper troposphere. These differences reflect significant uncertainties in the present global atmospheric water distribution, as well as how it is controlled and will vary in a changing climate. As such, these differences motivate much of the present work.

7.2. Humidity Comparison Overview

We begin our comparison of the GPS occultations and the other global analyses in terms of refractivity. Figure 15 shows the JJ95 zonal mean GPS minus ECMWF refractivity structure. Figure 16 shows the vertical structure of the globally averaged refractivity differences in Figure 15 as well as the analogous quantity for NCEP. The agreement in Figure 16 is quite close with a maximum GPS-ECMWF discrepancy of ~0.8% near 3 km altitude. The NCEP differences exhibit a relative maximum of ~1% near 3 km altitude as well as a larger maximum of ~1.5% near the surface, where few GPS-MET profiles reach (Figure 6a). Because the GPS profiles penetrate to lower altitudes at high latitudes (Figure 6b), the near-surface GPS-NCEP refractivity bias in Figure 16 primarily reflects high-latitude behavior, particularly the relatively large negative differences at high southern latitudes. Since refractivity differences translate to specific humidity differences, the generally lower GPS refractivities in Figure 16 imply generally lower GPS specific humidities.

Figures 17, 18, and 19 show the zonal mean specific humidity differences between the GPS-MET results and the interpolated JJ95 ECMWF analyses, interpolated JJ95 NCEP reanalyses, and the PO JJA climatology, respectively. In general, the large spatial scales of the zonal mean structures indicate the differences are systematic, not random.

In general, GPS results tend to be somewhat drier than the other three analyses. The GPS specific humidities are drier than the ECMWF moisture analyses below 6 km altitude (~500 mbar), which is also reflected in the GPS-ECMWF precipitable water (PW) results in Figure 20. The GPS results are drier than the NCEP reanalyses through most of the troposphere with a notable exception between 10°S and 30°N in the lower troposphere. The GPS-NCEP PW differences are similar with negative values at almost all latitudes except the band between 5°S and 25°N (Figure 20). GPS results are generally drier than the PO results in the Southern Hemisphere and the northern subtropical free troposphere. Elsewhere however, the GPS results are generally moister than the PO JJA climatology.

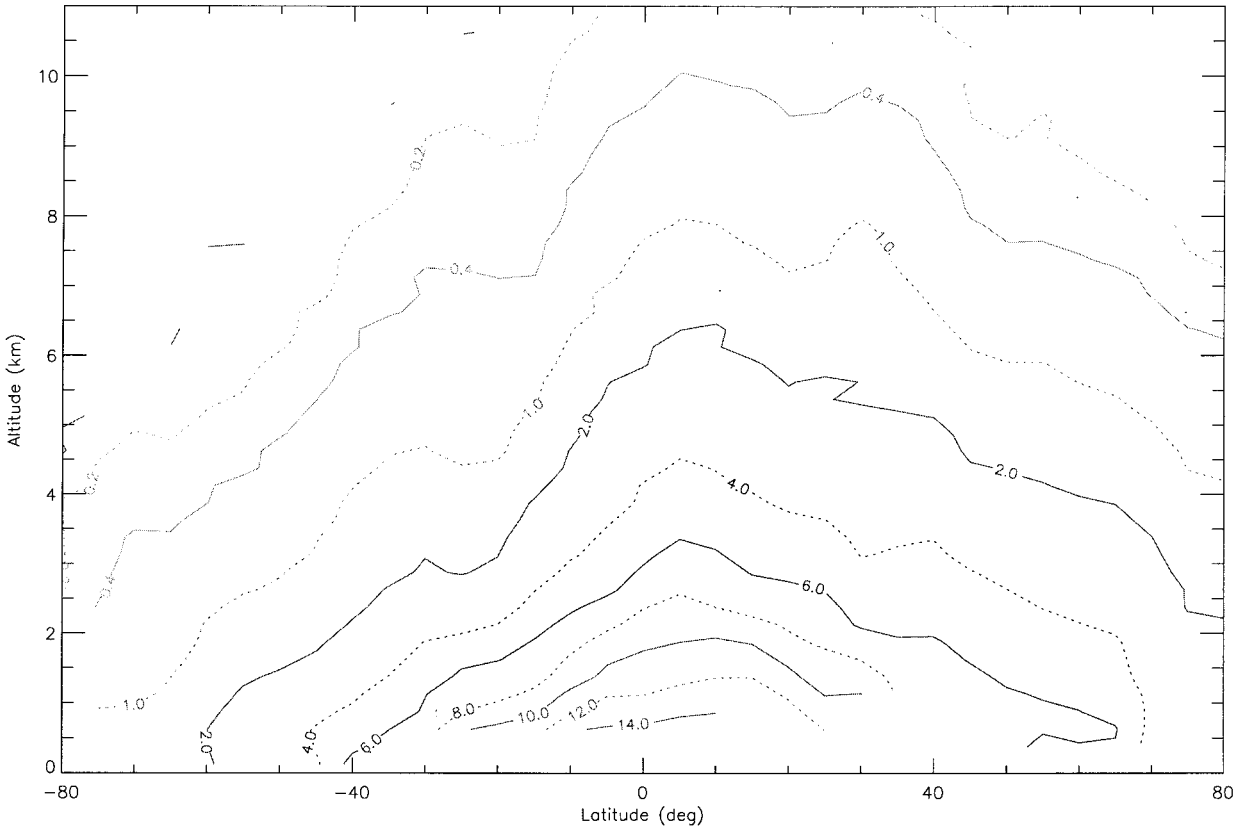

Figure 13. Average of zonal mean specific humidities: $\bar{q}_G$, $\bar{q}_{IE}$, and $\bar{q}_{IN}$, in g/kg.

7.3. Middle to High Southern Latitude Differences

The GPS zonal mean specific humidity estimates tend to be drier than the other three analyses through much of the Southern Hemisphere. GPS estimates are drier than the NCEP analyses by 0.4 g/kg or more over much of the high-latitude Southern Hemisphere below 4 km altitude and 30–50% drier than the NCEP and PO results through much of the free troposphere south of 30°S. Agreement between the GPS and the ECMWF zonal mean specific humidity estimates in this region is generally closer with differences more typically of the order of 0.1 g/kg.

While it is difficult to directly determine and assign errors in the Southern Hemisphere without an absolute global moisture standard, we can make some relevant comments. During JJ95 the Southern Hemisphere, as the winter hemisphere, contained far less water vapor than the Northern Hemisphere (e.g., Figure 13). As a result, since the GPS zonal mean moisture errors are expected to be of the order of ~0.1 g/kg (sections 3 and 6), the fractional errors in Southern Hemisphere GPS zonal mean moisture estimates will be larger than those in the Northern Hemisphere. GPS specific humidity errors due to temperature errors are presumably larger in the Southern Hemisphere based on Figure 10 and the relatively high temperature errors at high southern latitudes implied by negative zonal mean relative humidities there, as discussed in the Appendix.

The nonspherical refractivity structure associated with the relatively large horizontal temperature gradients in the winter hemisphere will lead to refractivity errors. However, the low wintertime specific humidities will contribute relatively little to the nonspherical refractivity structure. As a result, the horizontal refractivity variations will be dominated by temperature variations and, because of hydrostatic and geostrophic balance, will therefore be large scale in general. Consequently, we do not expect the nonspherical errors at middle and high southern latitudes to be especially large, at least away from weather fronts. Even the horizontal refractivity variations across wintertime fronts are surprisingly small. This is because refractivity on the cold side of a winter front has a higher dry density or hydrostatic contribution but a lower moist contribution (see (1)), whereas on the front's warm side the smaller dry contribution is compensated for by a larger moist contribution [*Kursinski et al.*, 1993]. Therefore we expect that the estimated refractivity errors due to horizontal refractivity gradients discussed briefly in section 3 are generally representative at middle and high southern winter latitudes.

One advantage of the small wintertime specific humidities is the lack of moisture allowed GPS occultation profiles to systematically extend to lower altitudes such that most profiles south of 40°S penetrated to within 0.5 km of the surface (Figure 6b). As a result, the GPS profiles have sampled most of the vertical extent of the southern troposphere and provided relatively high vertical resolution within and below the clouds that cover large portions of that hemisphere. In contrast, with extremely sparse and uneven radiosonde sampling over the largely remote Southern Hemisphere, the NCEP and ECMWF analyses must rely heavily on passive satellite radiances. The satellite radiance measurements provide limited vertical resolution amounting to 1–3 vertical moisture levels across the troposphere. The interpretation of the IR radiances, such as those from TOVS, is also confounded by frequent wintertime clouds. Error covariances and model physics must provide the additional constraints required to derive moisture and temper-

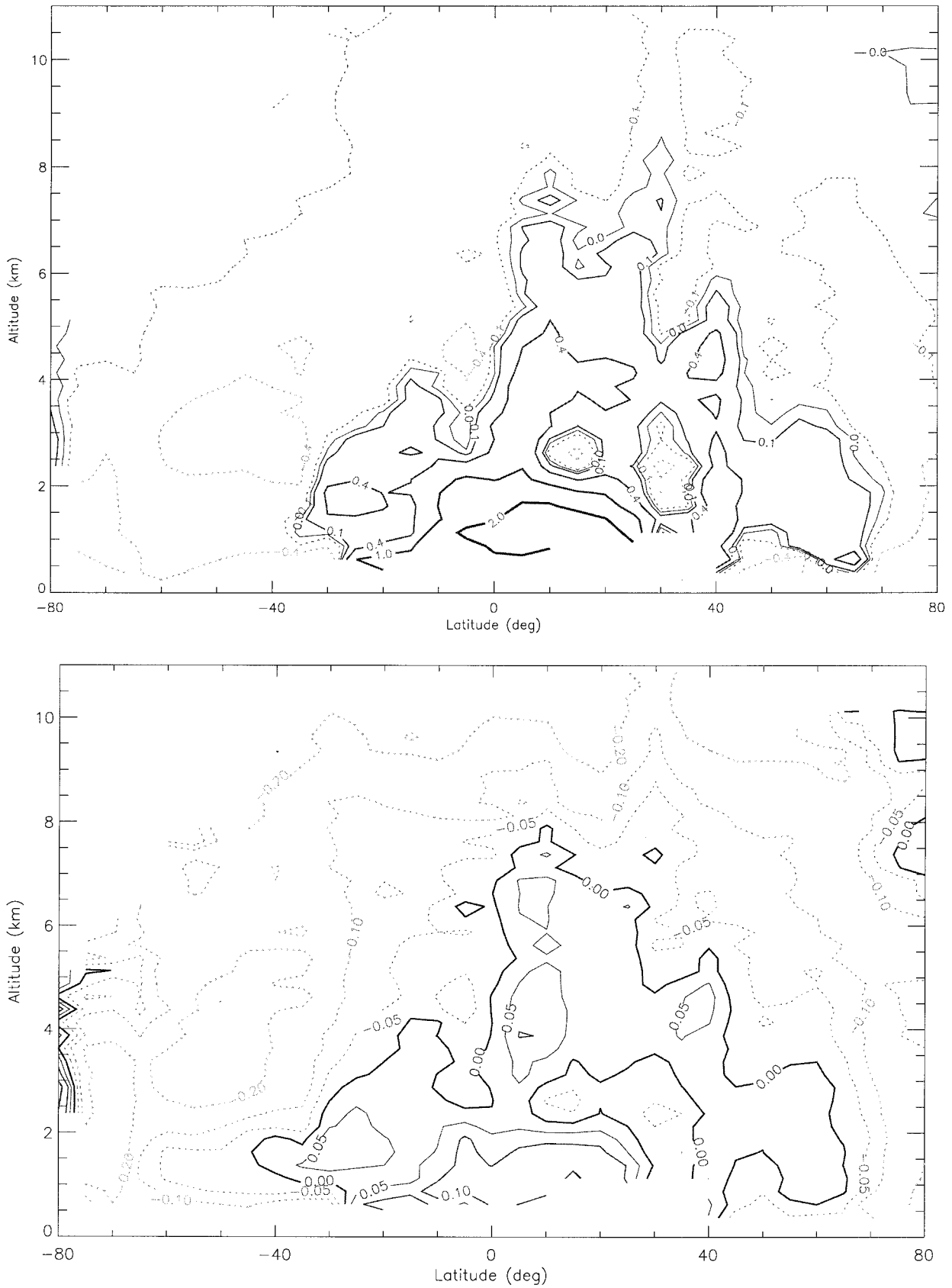

Figure 14. Differences between the ECMWF and the NCEP moisture analyses interpolated to the occultation locations. (top) Zonal mean specific humidity estimates ($\bar{q}_{\mathrm{IE}} - \bar{q}_{\mathrm{IN}}$) for JJ95. Contours are at 0, +0.1, +0.4, +1, and +2 g/kg. (bottom) Zonal mean relative humidity estimates ($\bar{U}_{\mathrm{IE}} - \bar{U}_{\mathrm{IN}}$) for JJ95. Contours are at 0, +5, +10, +20, and +40%.

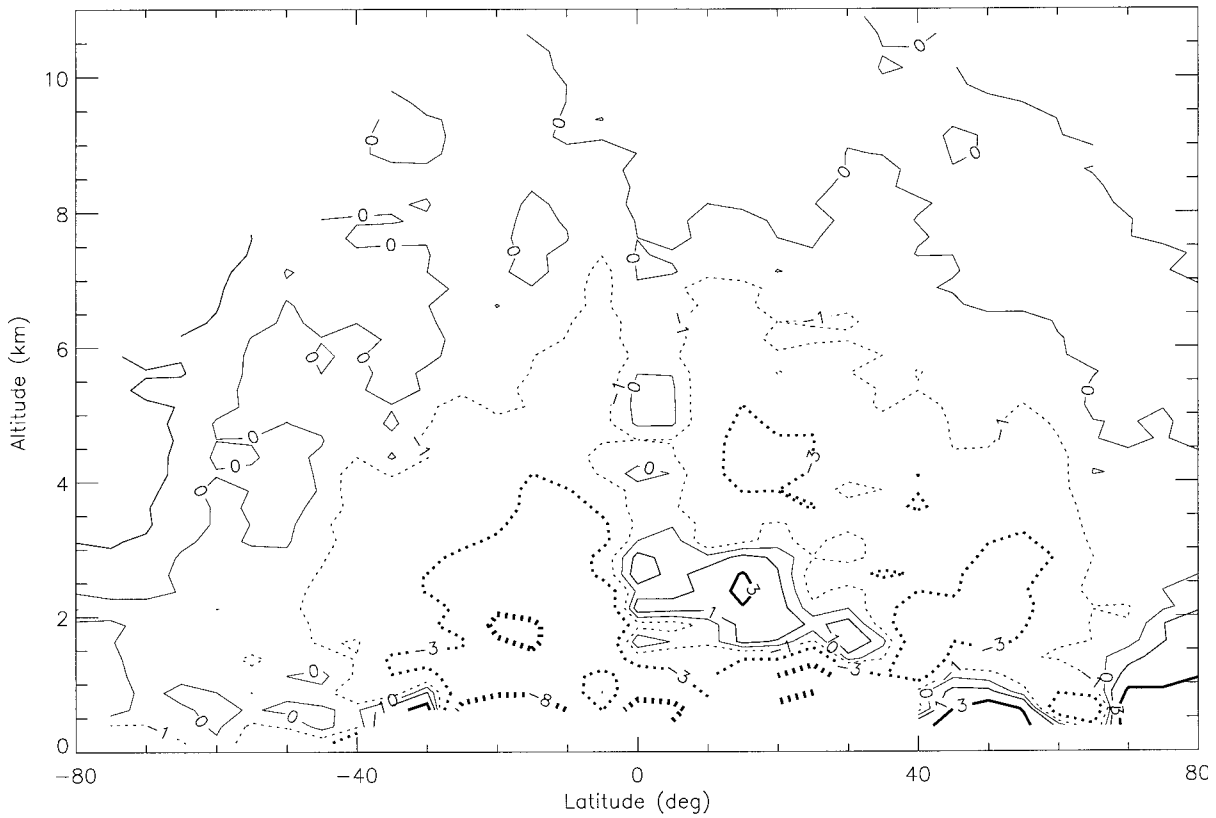

Figure 15. Differences between the zonal mean occultation refractivity estimates and the ECMWF analysis refractivity estimates ($N_G - N_{IE}$) for JJ95. Contours are 0, +1, +3, +8 N-units.

ature solutions at each analysis grid point. The classic PO climatology relies almost entirely on the extremely limited radiosonde sampling in the Southern Hemisphere combined with additional physical constraints to fill in the huge unsampled regions. Therefore, of the four moisture analyses, the GPS results may represent the most direct measurement of the true atmospheric behavior in the Southern Hemisphere, albeit with the limited sensitivity of GPS to the small water vapor concentrations found there.

On the basis of these arguments we suspect that the GPS zonal mean specific humidities in the Southern Hemisphere are probably accurate to 0.1 to 0.2 g/kg. Most of the GPS-ECMWF differences in the southern middle and high latitudes fall within this range and therefore appear to be consistent within the estimated GPS accuracy limits. Much of the GPS-NCEP specific humidity differences are larger, and the JJ95 NCEP results in the Southern Hemisphere may be somewhat moist-biased. This line of reasoning also implies that the moist GPS feature near 70°S and 5 km altitude above Antarctica is too small in magnitude to be significant and reliable.

7.4. Middle to High Northern Latitude Differences

The GPS humidity profiles capture the high specific humidities in the northern summer hemisphere evident in the other three analyses. Because of the higher specific humidities, GPS observational utility for moisture extends over a wider altitude range in the summer hemisphere. Approximately half of the GPS/MET profiles penetrate to within 1 km of the surface north of 40°N (Figure 6 (top)), yielding a good vertical coverage at these latitudes. In the lower and middle troposphere in the Northern Hemisphere, GPS results tend to be drier than the ECMWF and the NCEP reanalyses. North of 30°N, differences between the GPS results and the NCEP reanalyses are somewhat smaller than those between the GPS and the ECMWF analyses and range from +0.1 to −0.4 g/kg.

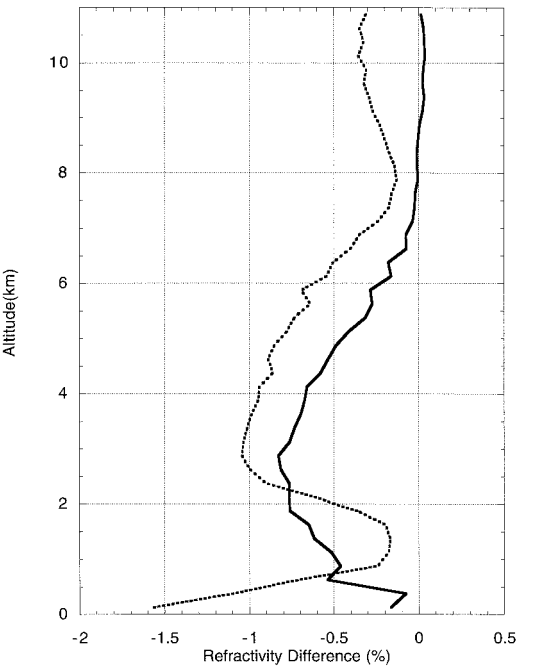

Figure 16. Vertical structure of the global mean, fractional refractivity estimate differences. Solid line, $N_G - N_{IE}$. Dashed line, $N_G - N_{IN}$.

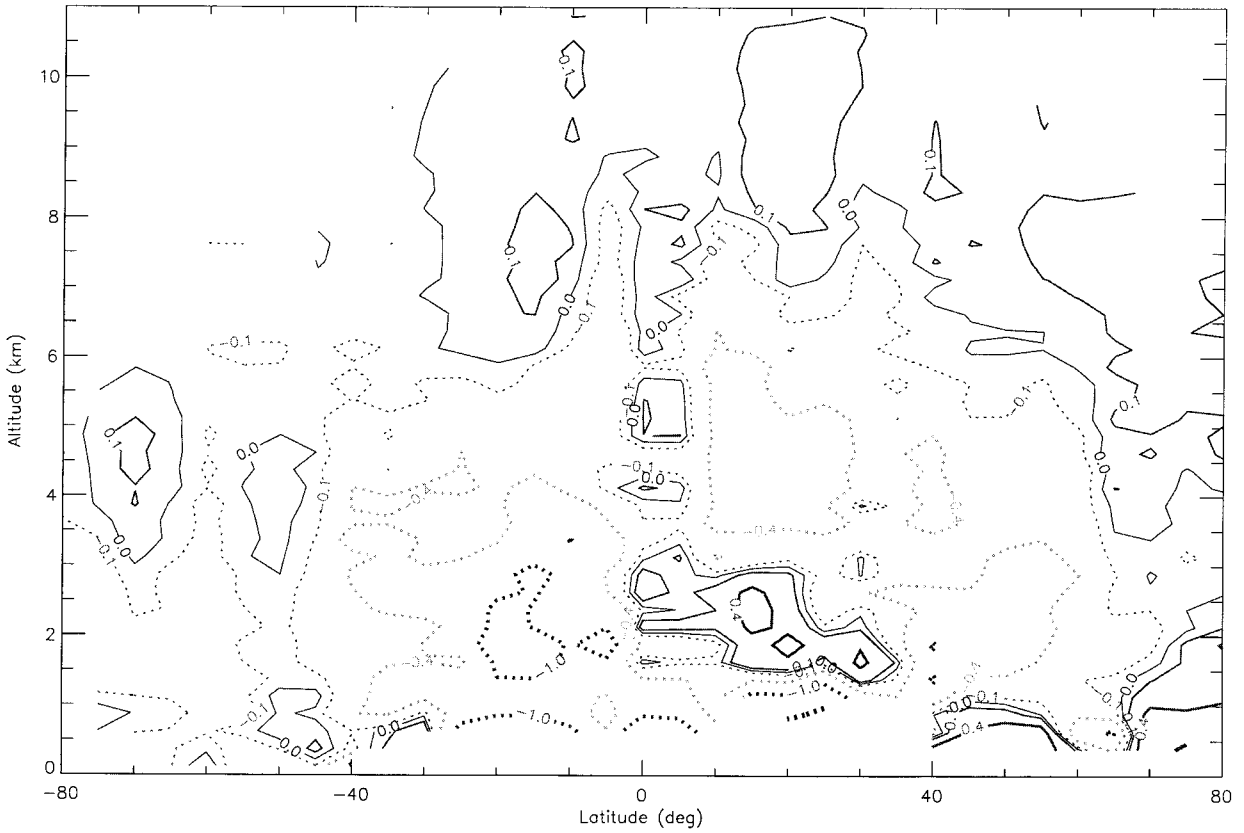

Figure 17. Differences between the zonal mean specific humidity estimates ($\bar{q}_G - \bar{q}_{IE}$) for JJ95. Contours are at 0, +0.1, +0.4, +1, and +2 g/kg.

The Northern Hemisphere GPS minus PO zonal mean specific humidity structure is more complex, exhibiting significant magnitude and sign variations in both altitude and latitude. Overall, the PO results tend to be drier than the other three data sets north of 35°N. The PO dryness may reflect interannual variability or trends such as increases in precipitable water (PW) over North America from 1973 to 1993 described by *Ross and Elliott* [1996] and *Elliott and Angell* [1997]. There may also be a bias resulting from the land-biased sampling of radiosondes used to derive the PO climatology.

7.5. High-Altitude Bias in the Northern Hemisphere

In the upper portion of the Northern Hemisphere north of 20°N, the GPS-ECMWF and GPS-PO zonal mean moisture differences are positive with similar magnitudes and spatial extents. The GPS-NCEP differences shows signs of a weaker signature of the same structure. Examination of the positive GPS-ECMWF bias in this region reveals that the bias is associated with a subtle difference between GPS and the ECMWF analysis pressures rather than refractivities which agree quite closely in this region (Figure 15). The cause of the pressure bias is uncertain, but it appears that the GPS moisture is overestimated because the mean relative humidity with respect to ice is near saturation such that the vapor would be supersaturated a large percentage of the time, which seems unlikely.

Because occultation-derived hydrostatic pressure is derived in a top-down manner, an underestimate of the occultation-derived hydrostatic pressures in the upper troposphere requires that occultation refractivities (and densities) must be underestimated in the lower stratosphere. The magnitude of pressure error required to produce a moisture bias of 0.1 g/kg is ~0.3% corresponding to a geopotential height error of ~20 m. The contribution of biases associated with initializing the Abel and hydrostatic integrals near 50 km altitude is too small to produce pressure errors of this order [*Kursinski et al*., 1997]. *Kursinski et al*. [1997] estimated that the biases in mean geopotential height of the upper troposphere would be ~1 m due primarily to horizontal structure, much less than the 20 m required error implying erroneous occultation retrievals are unlikely to be the dominant error bias.

Analysis pressures biased high in the upper troposphere could be the error source. Such errors would be caused by a combination of high surface pressure and high tropospheric temperatures. A scenario where ECMWF surface pressures are high on average by 0.3% (~3 mbar) is unlikely, particularly in the Northern Hemisphere. ECMWF analysis temperatures, which are warm throughout the troposphere by ~0.6 K, would cause the geopotential height of pressure levels in the upper troposphere to be too high by an amount consistent with the observed pressure bias. The error in refractivity associated with such a temperature bias would be zero approximately one scale height above the surface where the pressure and temperature error contributions to refractivity cancel, which is crudely consistent with the observed differences. Therefore the upper troposphere pressure discrepancies may be due to a positive tropospheric temperature bias in the analyses. If true, the location of such a bias in the Northern Hemisphere would further suggest that the temperature bias is tied to the radiosondes.

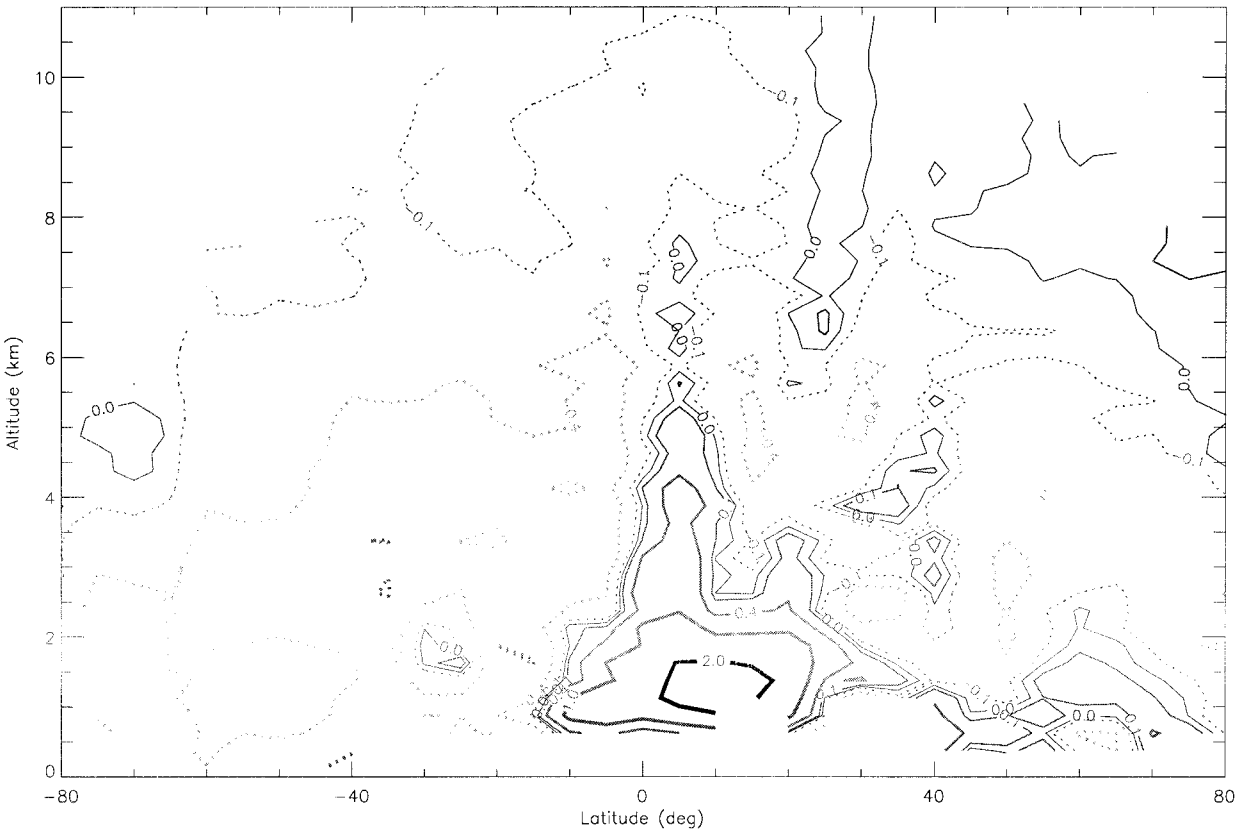

Figure 18. Differences between the zonal mean specific humidity estimates ($\bar{q}_G - \bar{q}_{IN}$) for JJ95. Contours are at 0, +0.1, +0.4, +1, and +2 g/kg.

7.6. Upper Troposphere Moisture Associated With Summer Monsoons

The JJ95 GPS, ECMWF, and NCEP zonal mean specific humidity estimates exhibit relative maxima near 30°N above an ~6 km altitude. The similar features of the maxima combined with a sharp decrease in specific humidity north of 40°N indicate the features are real, the result of moisture injected into the middle and upper troposphere by the summer monsoons in this latitude band. Indeed, the latitude-longitude distribution of the ECMWF-analyzed moisture field indicates that the highest specific humidities at 300 mbar (~9 km altitude) are associated with the Indian-Asian monsoon, not the ITCZ. The greater magnitude of the GPS and NCEP moisture estimates suggest more moisture is injected into the upper troposphere by the monsoons than the ECMWF and PO estimates. However, since the ~0.1 g/kg GPS-ECMWF difference is near the limit of expected GPS accuracy, it is difficult to draw conclusions about the relative accuracy of the different estimates.

7.7. Moisture Differences Near ITCZ

The low-latitude moisture differences vary significantly between Figures 17, 18, and 19. The difference structure in all three of the figures appears correlated with the tropical Hadley circulation. The GPS-PO zonal mean moisture differences between 30°N and 30°S exhibit the strongest correlation with moister GPS results centered roughly on 5°N coinciding with the ITCZ and drier regions to either side coinciding with the areas of large-scale subsidence. The low-latitude GPS specific humidity results agree most closely with those of ECMWF, particularly near the ITCZ where the differences are generally 0.1 g/kg or less in magnitude. In contrast, the GPS specific humidities are significantly wetter than both the NCEP and the PO results in the vicinity of the ITCZ below 7 km altitude and in the planetary boundary layer (PBL) from 10°S to 30°N. The contrast between the GPS-ECMWF and the GPS-NCEP differences are not surprising, given the significant low-latitude differences in Figure 14. The higher GPS and ECMWF zonal mean specific humidity estimates near the ITCZ are associated with a more sharply defined meridional maximum in the zonal mean moisture near the ITCZ. The meridionally smoother PO climatology may result from limited data near the ITCZ or simply variations over its 10 year averaging period. The meridional smoothness of NCEP reanalyses presumably reflects the heavy reliance of the NCEP moisture analyses on the NCEP model physics.

While only a limited number of GPS/MET profiles probe the low-latitude near-surface environment, Figures 17, 18, and 19 clearly indicate that large discrepancies exist between the ECMWF and the NCEP and PO results in this region. The maximum GPS minus NCEP and GPS minus PO differences reach more than 2 g/kg near 1 km altitude in the PBL region north of the ITCZ, representing fractional and relative humidity differences 10–20% lower than the GPS and ECMWF estimates. The striking similarity between the low-latitude structures of GPS-PO and GPS-NCEP differences in the lower troposphere (Figures 18 and 19) and their dissimilarity to the GPS-ECMWF structure (Figure 17) suggest that the PO and NCEP moisture analyses are both biased dry in this region. Somewhat surprisingly, the largest GPS-NCEP zonal mean differences in the PBL region are actually larger than the largest GPS-PO

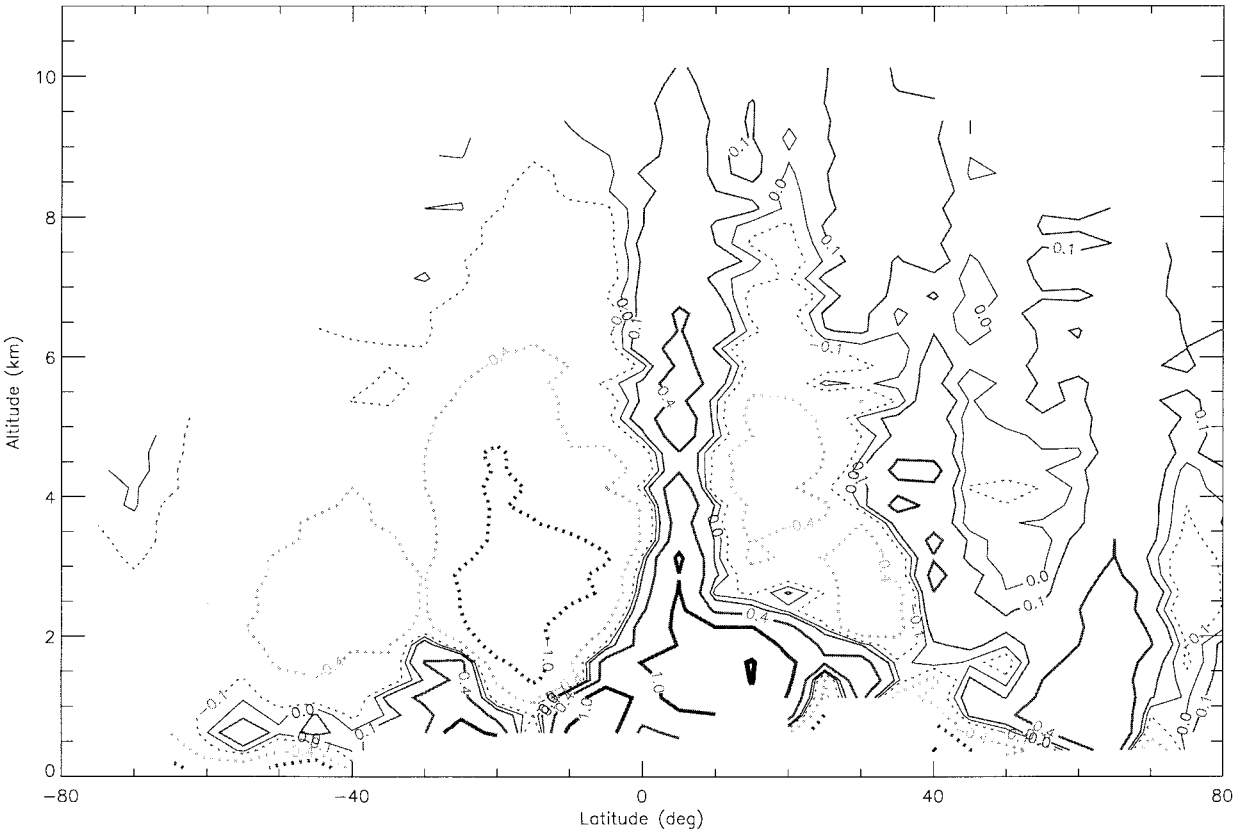

Figure 19. Differences between the zonal mean specific humidity estimates $\bar{q}_G$ for JJ95 and the Peixoto and Oort estimate of specific humidity ($\bar{q}_G - \bar{q}_{PO}$) for June-July-August (JJA). Contours are at 0, +0.1, +0.4, +1, and +2 g/kg.

differences, implying that recent humidity analyses can contain biases as large or larger than those generated from more limited data 30 years ago. The similar dry biases suggest that a common underlying model or physical parameterization problem may be responsible, causing both the NCEP and the PO analyses to inadequately resolve the meridional sharpness of the ITCZ and moisture concentrations in the nearby PBL. The significantly underestimated humidity near the ITCZ in the NCEP and PO results also suggests that the strength of the tropical Hadley circulation may be underestimated in these analyses as well.

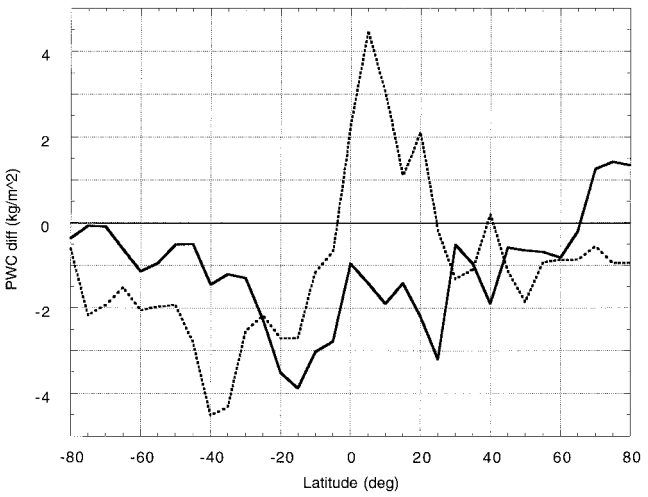

Figure 20. Differences in zonal precipitable water (PW) between the GPS humidity estimates and the ECMWF and NCEP humidity analyses for JJ95. Solid line, the vertical integral of the $\bar{q}_G - \bar{q}_{IE}$ differences in Figure 17. Dashed line, the vertical integral of $\bar{q}_G - \bar{q}_{IN}$ differences in Figure 18. Units are kg/m^2 or equivalently mm of precipitable water.

Above 6–8 km altitude and within 25° of the equator, the zonal mean GPS specific humidities are somewhat moister than the ECMWF results but somewhat drier than the NCEP results by similar amounts. The GPS results are wetter than the PO JJA climatology north of ~5°S but slightly drier to the south. The higher NCEP moisture estimates may be due to higher NCEP temperatures in this region. In general, these results are indicative of the uncertainty in upper tropospheric moisture amounts. GPS results in this region are consistent with both the NCEP and the ECMWF estimates to within the expected GPS errors and therefore provide little new information here.

7.8. Subtropical Differences

To the south and the north of the ITCZ in the free troposphere, zonal mean GPS-specific humidities are significantly drier than the other three moisture analyses. These areas coincide approximately with regions of low relative humidity in Figure 12 associated with the descending branches of the tropical Hadley circulation. The magnitudes and meridional structure of the zonal mean differences between the various analyses varies. The largest differences in the southern subtropics are between GPS and PO with the GPS zonal mean specific

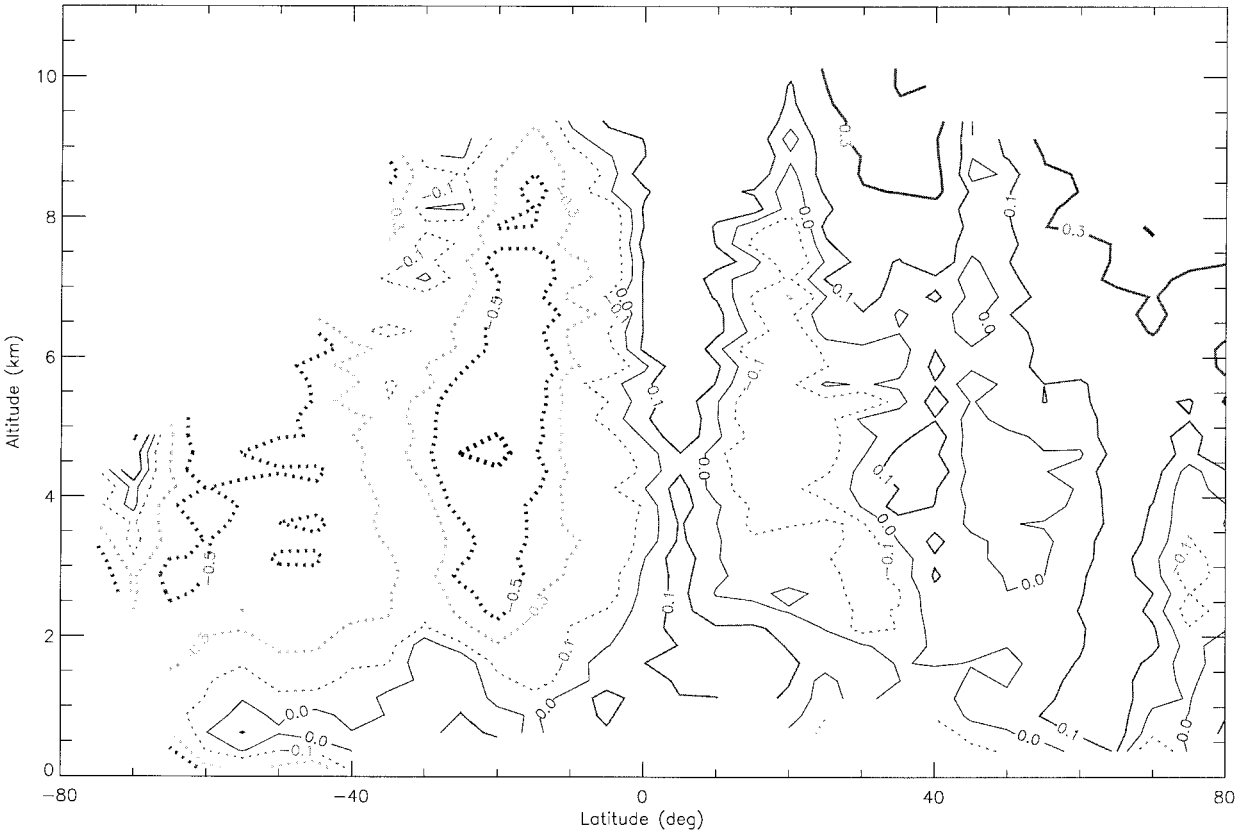

Figure 21. Fractional differences between the zonal mean specific humidity estimates $\bar{q}_G$ for JJ95 and the Peixoto and Oort estimate of specific humidity ($\bar{q}_G - \bar{q}_{PO}$) for June-July-August (JJA). Contours are at 0, −0.1, −0.3, −0.5, ±1.0.

humidities being drier than the PO results by more than 50% between 2 and 8 km altitude near 20°S (Figure 21). As discussed in section 7.10, a significant portion of the large GPS-PO differences are due to the positive bias in reported radiosonde humidities at low relative humidities.

In each of the three comparisons the location of the maximum GPS specific humidity dryness of ~1 g/kg relative to the other three analyses lies near 15°S–20°S and 2 km altitude. This location coincides approximately with the top of the convective PBL in the region of maximum subsidence. GPS refractivity and specific humidity profiles should, in general, be quite accurate in this region at least above the PBL because the subtropical free troposphere air is generally dry with relatively small horizontal temperature or moisture variations. Furthermore, the analyzed temperatures should also be particularly accurate because of generally small temperature variations here.

To understand why GPS results are systematically drier in this region, we examined individual profiles of GPS and ECMWF specific humidity near 20°S (Figure 22). These profiles reveal that the transition between the PBL and the free troposphere air is generally smoother and extends higher in the ECMWF analyses than in the GPS-MET profiles. In interpreting the cause of these differences, it is important to note that the sharp increase in temperature and decrease in moisture across the inversion capping the PBL both contribute to a large negative vertical refractivity gradient at the inversion height. This sharp gradient of refractivity intensifies atmospheric effects (such as bending) on an occulted signal, making it possible to accurately locate the inversion height despite the inability to directly separate the temperature and moisture contributions to the gradient. The large signal bending at the inversion height can even cause the loss of the signal (such as the case for many of the profiles in Figure 22), in which case the inversion height is well determined as the lowest height of the occultation.

These considerations suggest that the source of the dryness of the GPS results relative to the ECMWF results is systematic smoothing in the ECMWF analyses of the sharp vertical structure at the trade wind inversion. This conclusion is not surprising, given that much of the southern subtropics are remote oceanic regions devoid of radiosondes and that the TOVS resolution is inadequate to resolve the inversion structure. Furthermore, the 1-D-Var assimilation of TOVS data places little constraint on the 1.5–3.5 km altitude interval where the smoothing is observed [*McNally and Vesperini*, 1996, Figure 1], suggesting that the ECMWF analyses in this altitude regime rely heavily on the model physics. A reliance such as this can create a bias perhaps through a diffusive representation of the boundary layer entrainment process (D. Randall, personal communication, 1999).

The magnitude of the observed moisture bias near the trade wind inversion is probably larger than the bias of the ECMWF humidity analyses alone because the observed moisture bias includes errors in both $\bar{q}_G$ and $\bar{q}_{IE}$. The ECMWF moisture is probably overestimated just above the true inversion height because the PBL (and therefore PBL moisture abundance) in the analyses extends into what is in reality the free troposphere. The GPS zonal mean specific humidities are probably

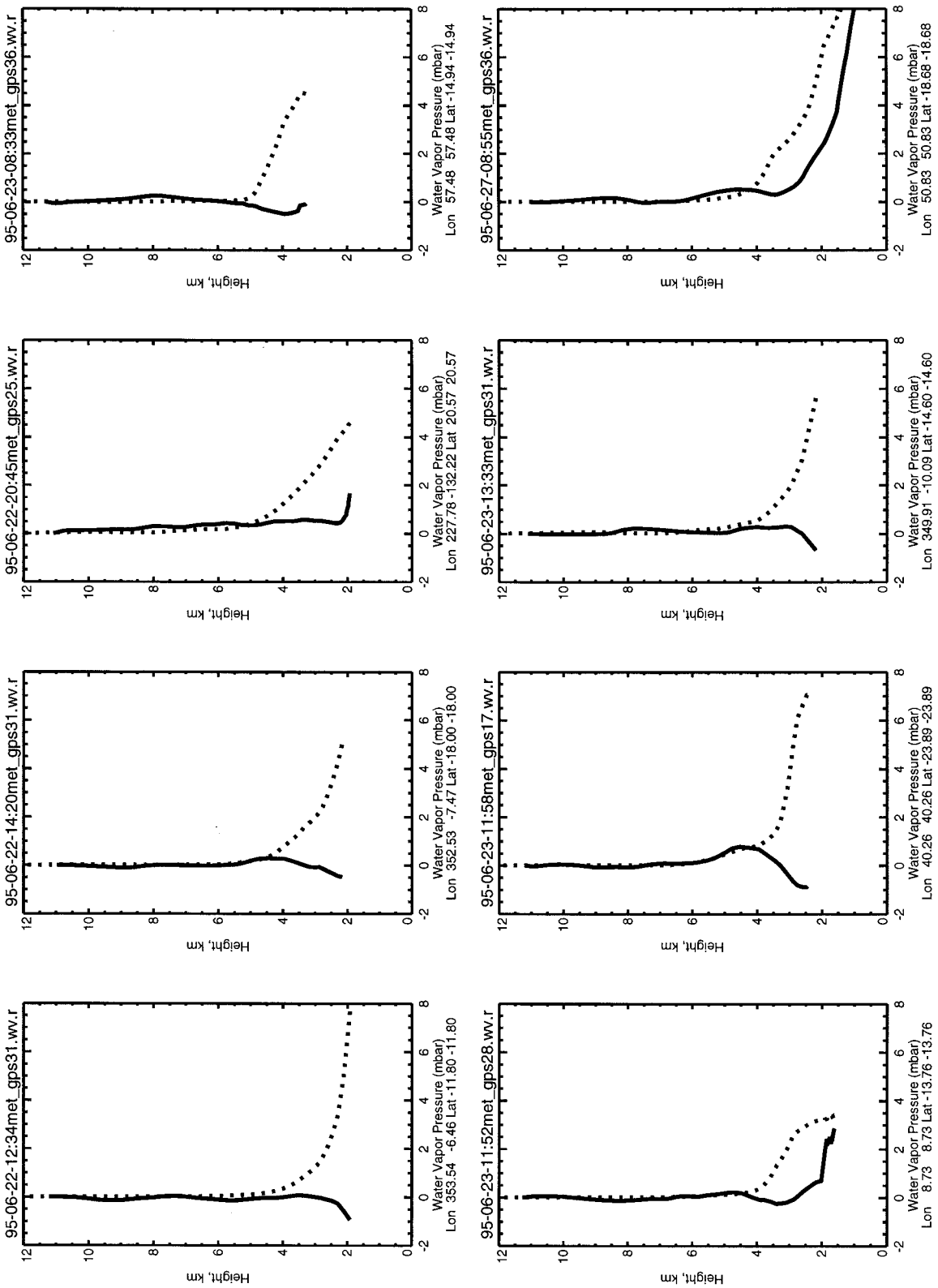

Figure 22. Examples of water vapor partial pressure profiles from subtropics for June 22 and 23, 1995, demonstrating the vertical structure of the bias between GPS profiles and ECMWF analyses. Solid lines are occultation-derived results. Dashed lines are profiles interpolated from ECMWF humidity analyses.

underestimated just above the true inversion height because the cooler PBL temperatures in the ECMWF analyses extend to heights that are in reality within the free troposphere. This cold bias effect is evident in several profiles of Figure 22, where the $\bar{q}_G$ reaches a minimum just above the trade wind inversion. A temperature bias of 4–5 K, representative of roughly half the temperature change across the inversion top, would cause $\bar{q}_G$ to be low by ~0.5 g/kg. Because the height of the inversion varies, the magnitude of the cold bias in the zonal mean estimate will be somewhat smaller. Therefore the 1–2 g/kg dry moisture bias near 20°S and 2 km altitude in Figure 17 probably overestimates the bias between the ECMWF humidity analyses and the truth by somewhat less than 0.5 g/kg. In the future a better estimate of the true moisture and moisture bias can be derived when analysis temperatures are adjusted in a 1-D-Var scheme or something analogous which combines the moisture and temperature analyses with the occultation refractivities. To function properly, such a scheme will have to account for the fact that the analysis errors are larger near the trade wind inversion.

The correspondence of the regions of negative bias to the descending branches of the tropical Hadley hints at a possible relation to the Hadley circulation. The largest moisture bias found near the top of the PBL may be the result of the analyses underestimating the strength of the tropical Hadley circulation, in general, such that the analyzed subsidence is not pushing downward against the PBL top as much as it is in reality.

7.9. Precipitable Water Differences

Figure 20 shows the GPS-ECMWF and GPS-NCEP zonal mean precipitable water content (PW) differences, which is the vertical integral of the specific humidity differences in Figures 17 and 18. The sign and magnitude of the $\bar{q}_G$ minus $\bar{q}_{IE}$ PW bias is similar to a bias found between columnar water from the ECMWF 1-D-Var reanalyses and those derived from collocated radiosondes over the period 1979–1993 [*Uppala*, 1997]. The moist bias in the ECMWF reanalyses was found to be as large as 2.4 mm relative to the sondes. The ECMWF humidity analyses are moister than the GPS results by as much as 3 mm in the subtropics (Figure 20).

As mentioned earlier, the subtropical GPS-ECMWF difference is probably somewhat overestimated due to the cold-biased temperature analyses just above the true tradewind inversion. It is interesting that the GPS-ECMWF PW bias and that between the ECMWF analyses and radiosondes are similar given that the present occultation profiles generally miss the lowest kilometer of the atmosphere where specific humidities are highest. If the GPS results are correct, there is not much difference between the sondes and the ECMWF in the lowest kilometer of the atmosphere. If not, the GPS results may be biased dry. Zonal differences will also exist simply because the radiosonde-ECMWF comparison is annual, while the GPS-ECMWF comparison only spans the JJ95 period. The consistency of the GPS versus ECMWF analysis comparison and that of the radiosonde versus ECMWF analysis comparison lends added credibility to the GPS results and suggests that the ECMWF moisture analyses are generally biased somewhat high.

The meridional dependence of the GPS-NCEP PW difference at low latitudes may partially reflect a bias in the TOVS-based vertically integrated water content produced operationally by the NOAA National Environmental Satellite Data and Information Service (NESDIS). *Wittmeyer and VonderHaar* [1994] found that the NESDIS TOVS retrievals systematically overestimated the column moisture in the subtropics and underestimated it in the tropics with respect to the Special Sensor Microwave Imager (SSM/I) results, generally consistent with the low-latitude GPS-NCEP PW differences in Figure 20.

7.10. Moist Peixoto and Oort Climatology Bias Due to Radiosondes

In the Southern Hemisphere the GPS zonal mean moisture estimates are generally smaller than those of PO. The greatest negative GPS-PO differences in the free troposphere are found near 20°S with absolute magnitudes greater than 1 g/kg near the trade wind inversion (~2 km). Expected GPS errors of ~0.1 g/kg, discussed in sections 3 and 6, are insufficient to explain much of the observed bias pattern. Furthermore, the GPS results agree more closely with those of ECMWF than with the PO JJA climatology. Since a large portion of this region contains zonal mean relative humidities lower than 20% (Figure 12) and since minimum reported radiosonde relative humidities have generally been truncated to 20%, it is not surprising that a large negative humidity bias should exist in this region. The correspondence of the location of maximum fractional dry $\bar{q}$ bias (>50%) near 5 km altitude to that of the minimum GPS zonal mean relative humidity (<10% relative humidity) is consistent with a positive relative humidity bias in the radiosonde data. Furthermore, comparable accuracy is expected of the GPS refractivity results in the Southern and Northern hemispheres suggesting the moisture bias does not result from a bias in the GPS refractivities. These facts suggest that the free troposphere in the Southern hemisphere during JJ95 is significantly drier than the JJA climatology of PO.

Since we cannot undo the radiosonde biases in the PO climatology, we have tried to gain some insight by limiting the minimum humidity of the GPS moisture profiles to 20% relative humidity ($= q_{G20}$). The resulting specific humidity differences, $\bar{q}_G - \bar{q}_{G20}$ and $\bar{q}_{G20} - \bar{q}_{PO}$, are shown in Figures 23 and 24, respectively. As expected, zonal mean moisture differences are greatest in the southern subtropics and are significant in the northern subtropics because these are the regions of lowest zonal mean relative humidity. Since the 0.1–0.4 g/kg increases in Figure 23 in the upper subtropical regions are comparable to the differences there in Figure 19, the $\bar{q}_{G20} - \bar{q}_{PO}$ differences are small and have become slightly positive above ~5 km altitude in the Southern Hemisphere and ~6 km in the Northern Hemisphere. The subtropics remain apparent in Figure 24 because regions where $\bar{q}_{G20} - \bar{q}_{PO}$ differences are still negative between 1 and 5 km altitude in the southern subtropics and between 2 and 6 km in the northern subtropics. There is little change between Figures 19 and 24 in the near-TCZ region of positive GPS-PO differences below 5 km altitude, indicating moisture in these regions seldom falls below 20% relative humidity.

Overall, the increase in the GPS-derived specific humidities produced by the 20% RH limit has reduced the difference between the GPS and the PO specific humidities. Figure 23 provides some indication of zonal mean biases present in the radiosonde data. Differences between Figures 19 and 24 indicate that the dry GPS-PO differences in the upper subtropical regions in Figure 19 probably contain significant contributions from the wet bias created by the 20% relative humidity truncation in the reported radiosonde data. It is also clear that the 20% truncation can only explain a portion of the differences in regions where the $\bar{q}_G - \bar{q}_{PO} < 0$ since the truncation elimi-

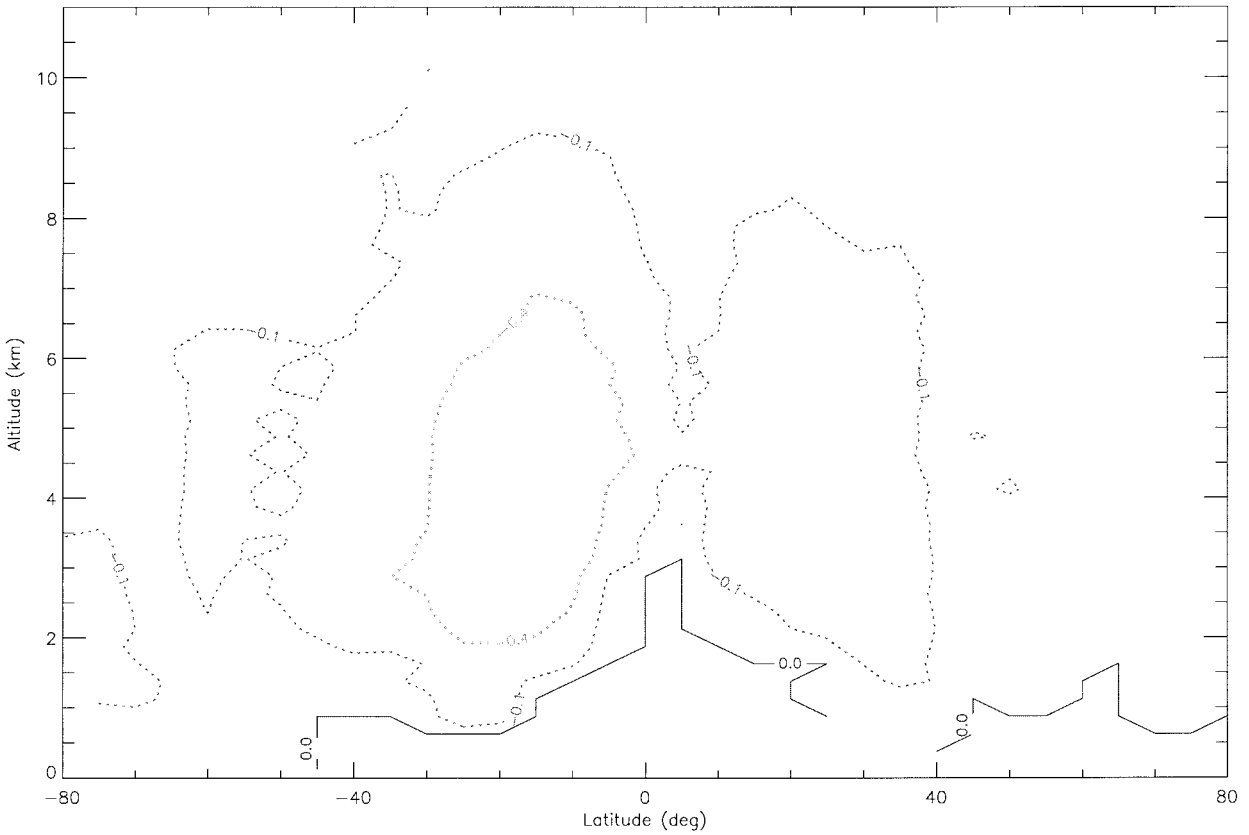

Figure 23. Differences between the zonal mean specific humidity estimates, $\bar{q}_G$ and $\bar{q}_{G20}$, where $\bar{q}_G$ is the zonal mean specific humidity shown in Figure 11 and $\bar{q}_{G20}$ is $\bar{q}_G$ modified by having each GPS moisture profile truncated to a minimum relative humidity of 20% before forming the zonal averages. Contours are at 0, +0.1, +0.4, +1, and +2 g/kg.

nated the bias only in certain regions. Several possible explanations for the behavior in Figure 24 include interannual variability, long-term trends, and biases due to spatial sampling biases, particularly in the PO climatology. The existence of drier GPS results even after the moistening associated with truncating to 20% minimum relative humidity allows the possibility of real drying of the lower portions of the subtropical free troposphere over the past 30 years. Given the importance of the subtropical moisture distribution in maintaining the Earth's radiative balance and the uncertainties that exist regarding the distribution [e.g., *Spencer and Bracewell*, 1997], such a possibility deserves serious consideration. The decrease in opacity associated with reduced moisture in the lower subtropical free troposphere would increase the radiation escaping from the PBL to space, representing a potentially important negative feedback in the climate system.

7.11. Planetary Boundary Layer Differences

It is tempting to overinterpret the GPS-PO differences within the PBL, particularly given that the magnitudes of GPS-PO boundary layer moisture differences near the ITCZ are similar to those reported in several studies of low-latitude radiosonde moisture trends [e.g., *Elliott*, 1995]. Unfortunately, any conclusions drawn from the present GPS-MET data regarding internal PBL behavior are premature because of the limited number of profiles that penetrate well into the boundary layer (see Figure 6 (bottom)). As a result, the zonal mean GPS estimates probably contain some bias at the lowest altitudes because the limited number of occultations probing well into the PBL may do so only under certain conditions. One might conclude that since this initial set of GPS occultations probes deeper into dry regions than wet regions that the GPS boundary layer results will be dry biased. However, occultations can probe well into the near-surface environment under extremely wet conditions, as demonstrated in Figure 5. The cause of the signal loss, which determines the lowest altitude of an occultation profile, is actually related more to how rapidly the moisture varies vertically than the absolute amount of moisture. Therefore the sign of any low-altitude moisture bias in the GPS results at low latitudes is unclear at present. We hope that with newer GPS receiver-tracking capabilities under development that tracking-occulted signals to the surface will become routine, enabling routine and all-weather probing of the PBL from space.

8. Summary and Conclusions

We have discussed the derivation of moisture from refractivity profiles retrieved from GPS occultations. We showed that moisture derived from refractivity is related more directly to specific rather than to relative humidity because refractivity essentially represents a molecule counter. Individual specific humidity profiles derived from occultations should have rms errors ranging from 0.2 g/kg in the drier regions of the troposphere to 0.5 g/kg or more in the more moist regions, where

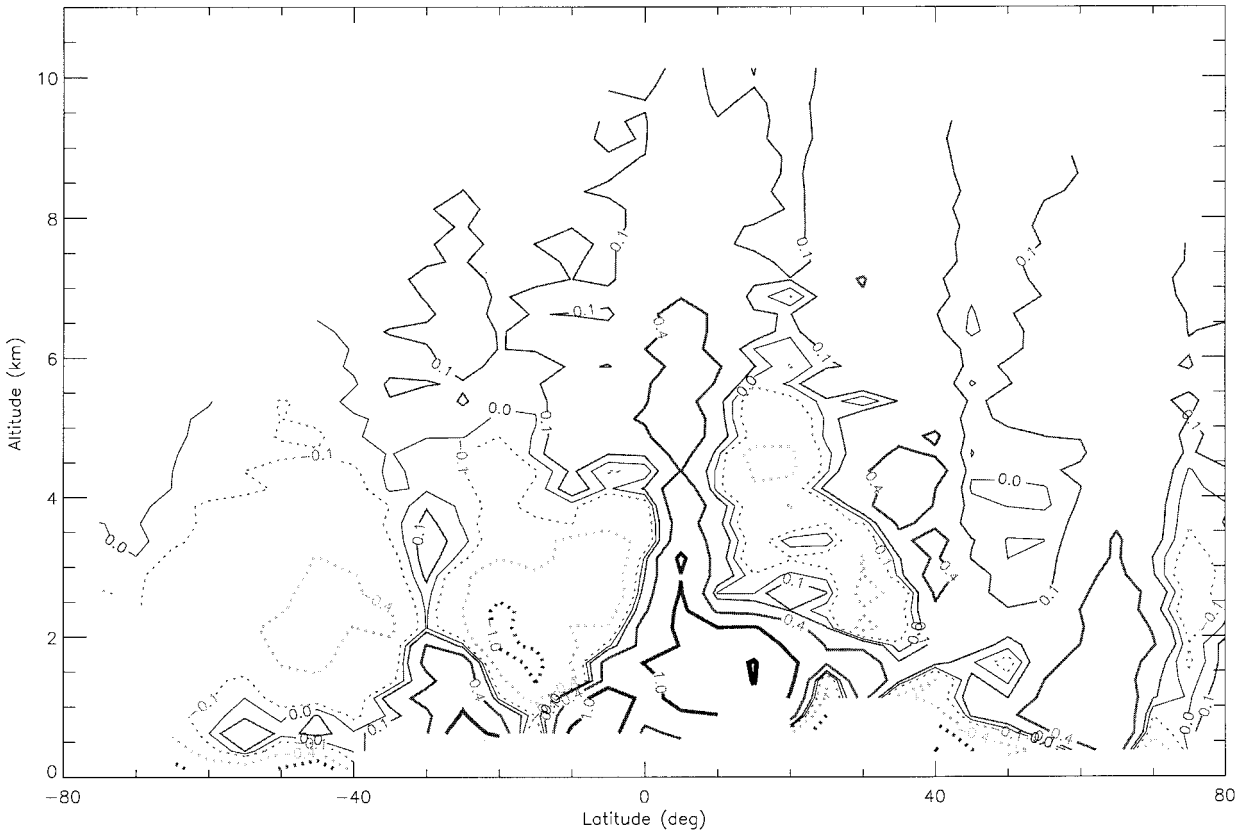

Figure 24. Differences between the truncated, GPS estimate of zonal mean specific humidity for JJ95 ($\bar{q}_{G20}$) and the Peixoto and Oort estimate of specific humidity ($\bar{q}_{PO}$) for June-July-August (JJA). Contours are at 0, +0.1, +0.4, +1, and +2 g/kg.

horizontal variations in humidity can cause larger errors in the refractivity profiles.

The bias or mean error in specific humidity should be accurate to about 0.1 g/kg limited by biases in assumed temperature. This prediction is consistent with the GPS comparisons with the ECMWF and NCEP moisture analyses as well as the differences between GPS specific humidity estimates caused by differences between the ECMWF and the NCEP temperatures in the middle and upper troposphere. Accuracy at low latitudes is probably somewhat better because of smaller temperature variability there. Since humidity derived from refractivity is absolute rather than relative, in regions where specific humidity is small, estimates of relative humidity derived from GPS results will be noisy and biased low. We found an extreme situation near 60°S above 5 km altitude where the mean-derived relative humidity is negative even though the mean specific humidity is positive, implying that the ECMWF analysis temperatures in the region are unusually noisy with an rms error of ~2.6 K.

To derive moisture, we used temperatures from global analyses together with the hydrostatic relation to estimate and remove the dry gas contribution to refractivity leaving the moist part as the residual. While this approach is suboptimal, a more complete and optimal approach that modifies the analysis temperatures requires knowledge of the error covariances and biases of both the background analysis and the refractivity observations. The simpler approach we have chosen recovers most of the information and derives moisture information from the GPS observations under drier conditions than a variational solution would because of the relatively small weight the error covariances would give to the GPS results under such conditions. While the individual GPS humidity profiles derived in this manner may be noisier than the variational solutions, zonally averaging them has allowed us to characterize underlying biases between the GPS and the analyzed moisture fields, which can be very important in climate research and precipitation forecasting.

We examined tropospheric water vapor derived from ~800 globally distributed GPS-MET occultation profiles acquired between June 21 and July 4 1995 using temperatures interpolated from 6 hour global ECMWF analyses and NCEP reanalyses. The moisture profiles extend from the 230 K temperature level to typically within 1–3 km of the surface. Several profile examples presented demonstrated the vertical coverage and resolution of the occultation profiles and general consistency between the occultation observations and the other measures of atmospheric humidity.

Zonal mean moisture derived from the 800 profiles exhibited basic climatological features, including the sharp decrease in specific humidity with altitude and the large specific humidity contrast between the summer and the winter hemispheres. A relative maximum in specific humidity in the middle to upper troposphere between 30°N and 40°N reflects the injection of moisture into the free troposphere by the summer monsoons. The signature of the tropical Hadley circulation is quite evident with maximum specific and relative humidity near the ITCZ and a minimum in relative humidity to either side coinciding with the subtropical zones of subsidence. The large

range of relative humidities observed across the subtropics and tropics is due almost entirely to variations in specific humidity because temperature variations across these zones are small. The asymmetry of the zones of minimum relative humidity in the Northern and Southern Hemispheres is consistent with the meridional asymmetry of the tropical Hadley circulation strength. The lowest relative humidities ranging from 10 to 20% are found near 20°S in the free troposphere coincident with the zone of the subsiding branch of the tropical Hadley circulation in the winter hemisphere.

The occultation moisture estimates are somewhat drier than the ECMWF global analyses below the ~260 K contour. The magnitude of the dry bias generally increases toward warmer temperatures except near 2 km altitude between 0° and 30°N, where the GPS results are slightly more moist than the analyses. The GPS results were generally drier than the NCEP moisture analyses except near the ITCZ and the PBL north of the ITCZ, where the NCEP reanalyses are significantly drier than either the ECMWF or the GPS moisture estimates. The largest dry bias of more than 1 g/kg near the trade wind inversion in the southern subtropics is associated with vertical smoothing of the inversion in the analyses. The similarity of the GPS versus ECMWF biases with comparisons between ECMWF and radiosondes and SSM/I suggest the ECMWF analyses are moist-biased and lend credibility to the occultation results.

In the middle to upper troposphere of the Northern Hemisphere the GPS results are significantly moister than the ECMWF and PO analyses but only slightly moister than the NCEP reanalyses. The fact that the GPS and NCEP mean humidities are close to saturation with respect to ice indicate they may be overestimated. An unusual aspect of the GPS bias relative to the ECMWF analyses is its association with a pressure (rather than refractivity) difference. While the cause is uncertain, its symptoms are somewhat consistent with a warm bias of ~0.6 K in the tropospheric analysis temperatures suggesting a possible radiosonde temperature bias. However, the smaller bias relative to the NCEP reanalyses, which also assimilate the radiosonde data, may suggest otherwise.

We found significant differences between the PO moisture climatology for JJA derived from 1963 to 1973 and that derived from the GPS and ECMWF moisture results for the JJ95 period. Several potentially significant contributions to these differences include natural variability, long-term trends, and measurement errors as well as spatial biases inherent in the PO climatology. The general coincidence of regions of dry biases and regions of low relative humidity suggests a moist radiosonde bias contributes significantly to the dry biases. The GPS and ECMWF results reveal a much wetter ITCZ than that in the PO JJA climatology that could reflect a moistening trend. However, the similarity of the GPS-PO and GPS-NCEP biases near the ITCZ, combined with much better agreement between the GPS and the ECMWF-ITCZ moisture estimates, suggest that the PO JJA moisture climatology and NCEP reanalyses have underestimated the near-ITCZ humidity probably associated with an underlying model bias.

Finally, it is important to point out that our comparisons and conclusions have involved the ECMWF forecasting and analysis system in ~1995. The ECMWF and NCEP systems improve significantly with time. The present ECMWF system includes significantly more model levels and a 4-D-Var assimilation scheme and assimilates additional data types such as SSM/I and ATOVS. We are therefore looking forward to intercomparison studies between the present-day global analyses and the data from the new orbiting GPS receivers as well as the eventual assimilation of the GPS data into the ECMWF, NCEP, and NASA Data Assimilation Office (DAO) analysis systems.

Appendix: Negative Mean Relative Humidity

Following *Kursinski et al.* [1995] and using the Clausius-Clapeyron relation, the estimated zonal mean relative humidity, including refractivity, pressure, and temperature errors, is

$$\tilde{\bar{U}} \overline{\frac{P_w}{P_w^*}\left(1 + B\left[\frac{\varepsilon_N}{N} - \frac{\varepsilon_P}{P} + \frac{\varepsilon_T}{T}\right]\right)} \cdot \overline{\exp\left[-b\left[\frac{\varepsilon_T}{T} - \left(\frac{\varepsilon_T}{T}\right)^2 + \cdots\right]\right]},$$

where P_w and P_w^* are the true water vapor partial pressure and saturation vapor pressure, $b = 0.622L/R_dT$, L is latent heat and R_d is the gas constant for dry air, $B = a_1TP/a_2P_w \cong a_1Tm_w/a_2qm_d$, ε_N is the error in the retrieved refractivity, ε_T is the error in the ECMWF temperature and ε_P is the error in the hydrostatic pressure estimate, and the overbar represents the zonal mean.

Expanding the temperature errors in the exponential to second order, and assuming that the true temperature variations are uncorrelated with the temperature, pressure, and refractivity errors, and the ECMWF temperature errors are uncorrelated with the GPS refractivity errors and pressure errors, yields

$$\tilde{\bar{U}} = \overline{\frac{P_w}{P_w^*}}\left[1 + \overline{B\left(\frac{\varepsilon_N}{N} - \frac{\varepsilon_P}{P}\right)} + \overline{(B-b)\frac{\varepsilon_T}{T}} + \overline{(-Bb + b + b^2)\left(\frac{\varepsilon_T}{T}\right)^2}\right]. \quad \text{(A1)}$$

The first term on the RHS of (A1) is the true $\bar{U}$ and must be positive. While the second and third terms representing contributions of mean errors in refractivity, pressure, and temperature can be negative, these terms will also cause $\bar{q}$ to be negative. The term, which will cause $\bar{U} < 0$ when $\bar{q} > 0$, is the $-Bb$ term in (A1), which is always negative. The conditions near 60°S and 5 km altitude where $\bar{U}$ and $\bar{q}$ are observed to be negative and positive, respectively, are approximately $\bar{q} = 0.1$ g/kg and $T = 235$ K. Under these conditions, b is ~26, and B is ~300 such that Bb is much greater than either b or b^2, and the contribution of the mean square temperature error in (A1) is indeed negative. The minimum mean square temperature error to make (A1) negative is approximately

$$\overline{\left(\frac{\varepsilon_T}{T}\right)^2} = \frac{1}{Bb}. \quad \text{(A2)}$$

On the basis of these conditions and (A2), 2.6 K is the minimum rms temperature error required to explain the negative mean relative humidities and positive mean specific humidities observed near 60°S. This is significantly larger than the more typical 1.5 K rms error. It is worth noting that q generally increases toward lower altitudes, causing B to decrease, while the temperature errors do not vary much with altitude. As a result, (A2) cannot be satisfied in regions where the true mean specific humidity is much greater than 0.1 g/kg.

Acknowledgments. The research described in this publication was performed at the Jet Propulsion Laboratory, California Institute of Technology, supported jointly by the National Aeronautics and Space Administration and the Integrated Program Office for the National Polar-Orbiting Operational Environmental Satellite System. We would like to thank the GPS-MET Principal Investigator, Randolph Ware, and program manager, Mike Exner, for access to the raw GPS-MET data and the ECMWF for access to their 6 hour global analyses. We would also like to thank Roger Saunders, John Eyre, and Sean Healy for helpful comments and suggestions regarding this and related work.

References

Elliott, W. P., On detecting long-term changes in atmospheric moisture, *Clim. Change*, *31*, 349–367, 1995.

Elliott, W. P., and J. K. Angell, Variations of cloudiness, precipitable water and relative humidity over the United States: 1973–1993, *Geophys. Res. Lett*., *24*, 41–44, 1997.

Eyre, J. R., G. Kelly, A. P. McNally, E. Andersson, and A. Persson, Assimilation of TOVS radiances through one-dimensional variational analysis, *Q. J. R. Meteorol. Soc*., *119*, 1427–1463, 1993.

Fjeldbo, G., A. J. Kliore, and V. R. Eshleman, The neutral atmosphere of Venus as studied with the Mariner V radio occultation experiments, *Astron. J*., *76*, 123–140, 1971.

Gurvich, A. S., and T. G. Krasil'nikova, Navigation satellites for radio sensing of the Earth's atmosphere, *Sov. J. Remote Sens*., *7*, 1124–1131, 1990.

Hajj, G. A., E. R. Kursinski, W. I. Bertiger, S. S. Leroy, T. K. Meehan, L. J. Romans, and J. T. Schofield, Initial results of GPS-LEO occultation measurements of Earth's atmosphere obtained with the GPS-MET experiment, in *Proceedings of the IAG Symposium on G1, GPS Trends in Precise Terrestrial and Spaceborne Applications*, Springer-Verlag, New York, 1996.

Kalnay, E., et al., The NCEP/NCAR 40-year reanalysis project, *Bull. Am. Meteorol. Soc*., *77*, 437–471, 1996.

Kiehl, J. T., and K. E. Trenberth, Earth's annual global mean energy budget, *Bull. Am. Meteorol. Soc*., *78*, 197–208, 1997.

Kursinski, E. R., and G. A. Hajj, Zonal variability of water vapor derived from the Global Positioning System occultation observations during June–July 1995, *J. Geophys. Res*., in press, 2000.

Kursinski, E. R., G. A. Hajj, and K. R. Hardy, Atmospheric profiles from radio occultation measurements of GPS satellites, in *Proceedings of the Conference 1935 of the International Society for Optical Engineering* (*SPIE*), *SPIE Pap. 1935-13*, Soc. for Opt. Eng., Bellingham, Wash., 1993.

Kursinski, E. R., G. A. Hajj, K. R. Hardy, L. J. Romans, and J. T. Schofield, Observing tropospheric water vapor by radio occultation using the Global Positioning System, *Geophys. Res. Lett*., *22*, 2365–2368, 1995.

Kursinski, E. R., et al., Initial results of radio occultation observations of Earth's atmosphere using the Global Positioning System, *Science*, *271*, 1107–1110, 1996.

Kursinski, E. R., G. A. Hajj, J. T. Schofield, R. P. Linfield, and K. R. Hardy, Observing Earth's atmosphere with radio occultation measurements using the Global Positioning System, *J. Geophys. Res*., *102*, 23,429–23,465, 1997.

Leroy, S. S., Measurement of geopotential heights by GPS radio occultation, *J. Geophys. Res*., *102*, 6971–6986, 1997.

McNally, A. P., and M. Vesperini, Variational analysis of humidity information from TOVS radiances, *Q. J. R. Meteorol. Soc*., *122*, 1521–1544, 1996.

Meehan, T. K., J. M. Srinivasan, D. J. Spitzmesser, C. E. Dunn, J. Y. Ten, J. B. Thomas, T. N. Munson, and C. B. Duncan, The TurboRogue GPS receiver, paper presented at the Sixth International Geodetic Symposium on Satellite Positioning, Ohio State Univ., Columbus, Ohio, March 18, 1992.

Peixoto, J. P., and A. H. Oort, *Physics of Climate*, 520 pp., Am. Inst. of Phys., New York, 1992.

Rocken, C., et al., Analysis and validation of GPS/MET data in the neutral atmosphere, *J. Geophys. Res*., *102*, 29,849–29,866, 1997.

Ross, R. J., and W. P. Elliott, Tropospheric water vapor climatology and trends over North America: 1973–93, *J. Clim*., *9*, 3561–3574, 1996.

Shine, K. P., and A. Sinha, Sensitivity of the Earth's climate to height dependent changes in the water vapor mixing ratio, *Nature*, *354*, 382–384, 1991.

Smith, E. K., and S. Weintraub, The constants in the equation for atmospheric refractive index at radio frequencies, *Proc. IRE*, *41*, 1035–1037, 1953.

Soden, B. J., and F. P. Betherton, Interpretation of TOVS water vapor radiances in terms of layer-average relative-humidities: Method and climatology for the upper, middle, and lower troposphere, *J. Geophys. Res*., *101*, 9333–9343, 1996.

Spencer, R. W., and W. D. Braswell, How dry is the tropical free troposphere?—Implications for global warming theory, *Bull. Am. Meteorol. Soc*., *78*, 1097–1106, 1997.

Starr, D. O'C., and S. H. Melfi (Eds.), The role of water vapor in climate, A strategic research plan for the proposed GEWEX water vapor project (GVaP), *NASA Conf. Publ. 3120*, 1991.

Thayer, G. D., An improved equation for the radio refractive index of air, *Radio Sci*., *9*, 803–807, 1974.

Tyler, G. L., Radio propagation experiments in the outer solar system with Voyager, *Proc. IEEE*, *75*, 1404–1431, 1987.

Uppala, S., Performance of TOVS data in the ECMWF reanalysis 1979–1993, *Tech. Memo. 233*, Eur. Cent. for Medium-Range Weather Forecasts Res. Dep., Reading, England, 1997.

Vorob'ev, V. V., and T. G. Krasil'nikova, Estimation of the accuracy of the atmospheric refractive index recovery from Doppler shift measurements at frequencies used in the NAVSTAR system, *Phys. Atmos. Ocean*, *29*, 602–609, 1994.

Waliser, D. E., and C. Gautier, A satellite-derived climatology of the ITCZ, *J. Clim*., *6*, 2162–2174, 1993.

Ware, R., et al., GPS sounding of the atmosphere from low Earth orbit—Preliminary results, *Bull. Am. Meteorol. Soc*., *77*, 19–40, 1996.

Wittmeyer, I. L., and T. H. VonderHaar, Analysis of the global ISCCP TOVS water vapor climatology, *J. Clim*., *7*, 325, 1994.

Yunck, T. P., G. F. Lindal, and C. H. Liu, The role of GPS in precise earth observation, paper presented at the *Symposium on IEEE Position, Location and Navigation*, Inst. of Electr. and Electron. Eng., Orlando, Fla., Nov. 29–Dec. 2, 1988.

G. A. Hajj and E. R. Kursinski, Jet Propulsion Laboratory, MS 238-600, California Institute of Technology, Pasadena, CA 91109-0899 (rob.kursinski@jpl.nasa.gov)

(Received January 19, 2000; revised June 29, 2000;
accepted July 5, 2000.)